0322

Final Report

SLIPPERY WHEEL DETECTOR EVALUATION

By: JOSEPH S. ECKERLE
ROBERT L. KIANG

Prepared for:

SOUTHERN PACIFIC TRANSPORTATION COMPANY
ONE MARKET STREET
SAN FRANCISCO, CALIFORNIA 94105

STANFORD RESEARCH INSTITUTE
Menlo Park, California 94025 · U.S.A.

STANFORD RESEARCH INSTITUTE
Menlo Park, California 94025 · U.S.A.

Final Report *October 1975*

SLIPPERY WHEEL DETECTOR EVALUATION

By: JOSEPH S. ECKERLE
ROBERT L. KIANG

Prepared for:

SOUTHERN PACIFIC TRANSPORTATION COMPANY
ONE MARKET STREET
SAN FRANCISCO, CALIFORNIA 94105

SRI Project 3921

Approved by:

FRED J. KAMPHOEFNER, *Director*
Engineering Sciences Laboratory

BONNAR COX, *Executive Director*
Information Science and Engineering Division

CONTENTS

55
55
58
61
63
65
66
69
73
73
73
75
75
77
78
83
97
103
125

ILLUSTRATIONS

67
68
80
85
86
90
92
94
101
109
114
117
119
123

TABLES

I INTRODUCTION

Between the time a railroad car is loaded with freight and the time it is unloaded at its destination, it may travel as part of several different trains. The task of transferring cars from train to train is accomplished at classification yards, located at strategic points in the rail network. A typical classification yard consists of a single input track at one end and one or more output tracks at the other end. Several parallel storage tracks connect the two. Trains enter the classification yard in a serial manner, and are assembled on the several storage tracks in parallel. The highest point in a gravity classification yard, known as the "crest" or "hump," is located on the input track, just ahead of the switches that feed the storage tracks. All tracks slope downhill from this point.

Pushed by a locomotive, trains to be classified enter the yard on the input track. As each car or cut of cars reaches the crest, it is uncoupled from the train and coasts downhill toward the storage tracks. The switches are set so that each car will coast to the desired storage track. Retarders are located along the storage tracks and press against the sides of the car wheels to slow the coasting cars to a safe coupling speed.

Certain contaminants on the wheels of railroad cars may reduce the effective coefficient of friction between the car wheels and the shoes of the retarders used in classification yards. The result is a reduced capacity of the retarder to decelerate the car. In the extreme case, the car would have minimum deceleration resulting in an excessive overspeed impact with other cars on a storage track. Such a case resulted in the recent explosion and fire at Southern Pacific's Houston classification

yard, which was caused by an extreme overspeed impact of a car with an epoxy coating on its wheels. The retarder was unable to furnish proper retardation, even in maximum retard position due to this wheel condition.[1]

A proposed control proceedure is to install a "slippery wheel detector" before the crest of the classification yard. This device would detect wheels with low friction and alert the yard crew and the automatic control system in the case of an automated yard. Any cars with slippery wheels would not be uncoupled at the crest, but would be handled under an exception proceedure under the control of a locomotive. This report describes the first phase of the development of such a detector.

II SUMMARY

A. Basic Concept

When a rolling wheel is being slowed by a retarder, the wheel experiences a retarding force in a direction opposite to the wheel's motion. By Newton's third law, the retarder must also experience a longitudinal force in the direction of the wheel's motion. By measuring this reaction force, one can determine the effectiveness of retardation. The slippery wheel detector is therefore envisioned to take the form of a short section of retarder having a length anywhere from 2 feet to 6 feet. The reason for using such a short length is twofold. One is that the retarder should act on one wheel at a time to minimize the error that might be caused by having adjacent wheels in the detector at the same time. A second reason is that a short retarder would mean a lesser load on the locomotive, which not only has to push the train up the hump but also through the slippery wheel detector.

In addition to the longitudinal force discussed in the previous paragraph, a retarder would experience other types of reactions from a passing wheel. These would include a torsion of the retarder beam, stresses on various members of the retarder, and vibration of the retarder.

It is possible that any of these phenomena could provide a practical indication of retarder effectiveness. Longitudinal force and twisting moment can be directly measured with load cells, but this measurement technique requires a fair amount of modification on an existing retarder. Strain gages mounted on the retarder can measure these loads indirectly and would be easier to install on a retarder. While longitudinal force and twisting moment are considered to be the most direct indications of

retarder effectiveness, transducers for measuring vibration would be the easiest to install.

B. Description of Tests

To evaluate each of the above measurement techniques, three types of retarder instrumentation were tested:

(1) A load cell was mounted so as to measure directly the total retardation force. A method of mounting the load cell was devised that minimizes the sensitivity of the load cell to forces or moments other than those caused by wheel friction.

(2) Strain gages were mounted at various locations on the retarder to measure retardation loads in the retarder. The locations of the strain gages were carefully chosen to minimize response to loads other than those due to wheel friction and to maximize the signal-to-noise ratio.

(3) An accelerometer was mounted on the retarder to measure vibration.

The test apparatus is shown schematically in Figure II-1. To test the concept, a number of cars were pushed through the instrumented retarder and transducer output signals were recorded on magnetic tape for subsequent analyses. Slippery wheels were simulated by coating the wheels and retarder with lubricants.

C. Results and Conclusions

The test results indicate that the load cell would probably be the best instrumentation scheme--of the four schemes tested--for slippery wheel detectors. Strain gages mounted on the detector lever arms (see Section IV) could be used instead of the load cell and certain disadvantages of the load cell instrumentation scheme would be avoided. Unfortunately, the strain gage instrumentation scheme is less accurate than the load cell; in other words, more "false alarms" are expected from a

FIGURE II-1 TEST APPARATUS

strain-gage detector. A false alarm is an alarm given for a car that would decelerate normally in the yard's retarders.

Two other instrumentation schemes investigated--strain gages on the detector support casting (see Section IV) and an accelerometer mounted on the detector shoe--are even less accurate than either the load cell or strain gages on the lever arms and have no redeeming advantages.

From the test data, it appears that an excessive number of false alarms would be given if a minimum configuration slippery wheel detector, similar to the one used in the field tests, were employed in an active classification yard. Several improvements to this minimum configuration are suggested that should reduce the number of false alarms to an acceptable level and thereby provide a feasible slippery wheel detector system.

Another important parameter of a slippery wheel detector is the probability of "missed alarms." A missed alarm occurs when no alarm is generated for a car with slippery wheels where retarder effectiveness is impaired. To ensure the efficiency and reliability of the slippery wheel detector, a low probability of missed alarms must be demonstrated. This problem is discussed in relation to the design of slippery wheel detector tests for future phases of detector development.

III ANALYSIS OF RETARDER FUNCTION

A. Normal Functioning

Under normal conditions, the friction coefficients between the retarder shoe and wheel rim and between the wheel tread and running rail are both relatively high. Under these conditions, the wheel rolls without slipping on the running rail and the analysis of Appendix A gives the force, F, and moment, M, exerted on the retarder shoe. By Newton's third law, the loads exerted on the wheel rim by the retarder shoe will be equal to a -F and -M, about the wheel-rail contact point Q.

Figure III-1 is a view of the wheel showing all x-direction forces and z-axis moments acting on it. In this analysis, the effects of only

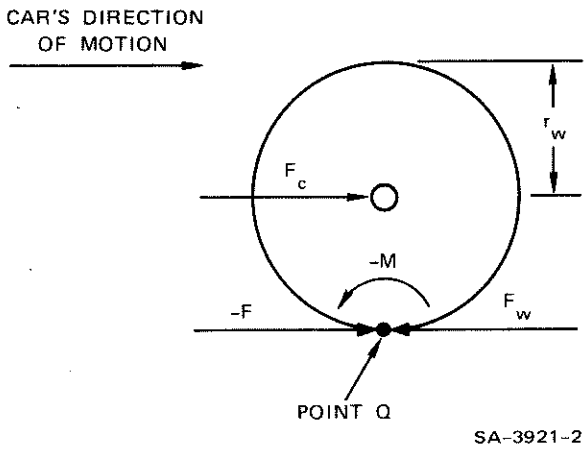

FIGURE III-1 WHEEL WITH FORCES AND MOMENTS ACTING ON IT

one shoe are being considered. In addition to loads from the retarder shoe, there is a force, F_W, exerted by the running rail, and a force, F_c, exerted on the wheel bearing by the car. Static equilibrium requires that

$$-M - F_c \, r_w = 0 \tag{1}$$

$$-F - F_w + F_c = 0 \tag{2}$$

where r_w is the radius of the wheel. The solution for Eqs. (1) and (2) is

$$F_c = \frac{-M}{r_w} \tag{3}$$

$$F_w = -F - \frac{M}{r_w} \tag{4}$$

By Newton's third law, the retarding force exerted on the car, F_R, is just $-F_c$. Using Eqs. (8) and (9) of Appendix A gives:

$$F_R = -F_c = \frac{-\mu N(K_M)}{r_w} \tag{5}$$

where μ is the friction coefficient and N is the normal force between the retarder shoe and wheel tread, and K_M is a constant that depends only on wheel and retarder geometry.

B. Slippery Rims or Retarder Shoes

In the presence of contamination, the coefficient of friction, μ, between the wheel rims and retarder shoes may be decreased. In this case, Eq. (5) still holds, and the decrease in retardation force, F_R, is proportional to the decrease in μ.

C. Slippage Between the Wheel and the Running Rail

Contaminants on the running rail or wheel tread could reduce the friction coefficient between the wheel and the rail to the point where the wheel no longer rolls without slipping. Cars have been lifted off the running rail while in the retarder. In this case, there is obviously a departure from pure rolling motion also. When a wheel slips on the running rail, the assumptions leading to Eqs. (8) and (9) of Appendix A are invalid. Hence, Eq. (5) is also invalid.

For the case where either the wheel has been lifted from the running rail, or the friction between the wheel tread and running rail is very small, we have

$$F_W \cong 0 \tag{6}$$

Solving Eqs. (1) and (2) with this constraint gives

$$F_R = -F_c = -F = M/r_w \tag{7}$$

Table III-1 summarizes the relations between the indicator of retarder performance, F_R, and the parameters F and M, which will be measured with the load cell and strain gages. These relations are derived from equations of this section and Appendix A.

Referring to Table III-1, the moment, M, is a better measure of retarder performance than the force, F. The relation between M and F_R does not depend on whether or not there is pure rolling motion of the wheel on the running rail. The relation of M to F_R depends on the wheel radius, but wheel radii vary from 14 inches to 19 inches, a variation of only ±15 percent from the mean. Up to a ten-fold decrease in retardation is expected when a slippery wheel is encountered, so the relatively small variations in wheel radii should be unimportant.

Table III-1

RELATIONS BETWEEN F_R, M, AND F

	Rolling Motion ($F_W \neq 0$)	Not Rolling Motion ($F_W \cong 0$)
In terms of F	$-F\left(\frac{K_F r_W}{K_M}\right)$	$-F$
In terms of M	$\frac{M}{r_W}$	$\frac{M}{r_W}$

Relating the force, F, to retardation is more problematic. Referring to Table III-1, the relation between F and F_R depends on whether or not the wheel is rolling on the running rail. The proportionality constant between F and F_R varies from -1 for $F_W \cong 0$ to

$$-\left(\frac{K_F r_W}{K_M}\right)$$

for pure rolling motion. K_F is a parameter, defined in Appendix A, that depends only on wheel and retarder geometry. The values of this proportionality constant for various wheel radii and rim geometries are:

	r_w = 14 in	r_w = 19 in
Outer rim	-1.22	-1.65
Inner rim	-0.69	-0.93

The variation in this constant is ±28 percent from the mean, which is still small compared to the ten-fold decrease in F_R expected for the most slippery wheels.

IV DESIGN OF STRAIN GAGE MOUNTING

A. Design Considerations

A strain gage is a device whose electrical resistance, R, is a function of its mechanical strain, ϵ. The relation is

$$F = R_o \left[1 + \epsilon(G.F.)\right] \qquad (1)$$

where R_o is the nominal gage resistance, and G.F. is the "Gage Factor," which is a property of the gage. For measurement of strain in load-carrying structures, strain gages are cemented to the structure. The strain of the gage is then equal to the strain in the structure at the location of the gage, and Eq. (1) relates the gage resistance to the strain in the structure.

Figure IV-1 is a schematic of a "two-gage bridge" circuit employing two strain gages, R_1 and R_2. Strain gages mounted on the retarder are

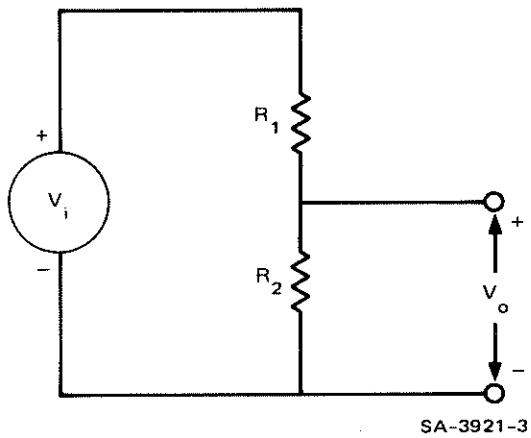

FIGURE IV-1 TWO-GAGE BRIDGE CIRCUIT

connected as in Figure IV-1. The gages are mounted so that the loads of interest cause equal and opposite strains in gages R_1 and R_2. The output voltage, V_o, of the circuit of Figure IV-1 is derived in Appendix B:

$$V_o = \frac{V_i}{2}[1 + \epsilon_2(G.F.)] \quad , \tag{2}$$

where ϵ_2 is the strain in R_2. In practice, the minimum strain that can be resolved is limited by the input noise inherent in the instrument used to measure V_o; thus,

$$\epsilon_r \cong \frac{2V_N}{(G.F.)V_i} \tag{3}$$

where ϵ_r is the resolvable strain and V_N is the instrument input noise voltage.

For strain gages to be effective, the resolvable strain, ϵ_r, should be much less than the minimum strain being measured. Referring to Eq. (3), ϵ can be reduced by increasing V_i or G.F. Input voltage, V_i cannot be increased indefinitely, because the power dissipated in the gages increases as V_i is increased. Power dissipation must be limited or the gages will be destroyed. The gage factors of foil strain gages are approximately 2, while the gage factors of semiconductor gages are 100 to 150. This is reflected in Table A-1 (Appendix A) which lists the dynamic range for foil and semiconductor gages mounted on the retarder at locations described below. The resolution of foil gages would be marginal for this application, so the decision was made to employ semiconductor strain gages for retarder instrumentation.

The strain gage responds to strain, regardless of the cause of the strain. For this reason, care must be exercised to ensure that phenomena that are not of interest do not cause strains which are indistinguishable from strains caused by the loads of interest.

Temperature changes of the retarder cannot be avoided and these will cause thermal strains to which the strain gages will respond. It is shown in Appendix B that the bridge connection of Figure IV-1 results in the output voltage, V_o, being insensitive to thermal strains.

Strain gage locations described below have been chosen so that the gages will respond to strains caused by retarder loads F and M (see Appendix A). Other retarder loads can cause strains at the gage locations that might be indistinguishable from strains caused by F and M. This problem is addressed in Appendix A where it is shown that the bridge connection of Figure IV-1 makes the output voltage, V_o, insensitive to retarder load, N.

B. Gages Mounted on Lever Arm

Strain gages were mounted on the retarder lever arms at locations A and A′. (See Appendix A, Figure A-4.) The gages were connected in a bridge circuit similar to Figure IV-1. Output voltages of the bridges should be proportional to F_{1x} and F_{2x} for gages on levers 1 and 2, respectively.

Lever arm pivots have been modified as described in Section V, "Design of Load Cell Mounting" to minimize friction. In Appendix A it has been assumed that the pivot friction is indeed small, which leads to Eq. (15), Appendix A:

$$F_{1x} = -F \quad . \qquad \text{(App. A, Eq. 15)}$$

If the pivot friction is not small, then the above equation becomes

$$F_{1x} + F_{2x} = -F \quad . \qquad (4)$$

Strain gages were mounted at locations A and A′ on both lever 1 and lever 2. Signals from the two levers were recorded separately and later compared to determine the effect of pivot friction.

C. Gages Mounted on Support Casting

Strain gages were mounted on the support casting at locations B and B′, Figure IV-2. The gages are connected in a four-gage bridge circuit described in "Design of Instrumentation" and in Appendix B. This connection results in an output voltage that should be proportional to the sum of the loads on each bracket. The analysis of Appendix A assumes

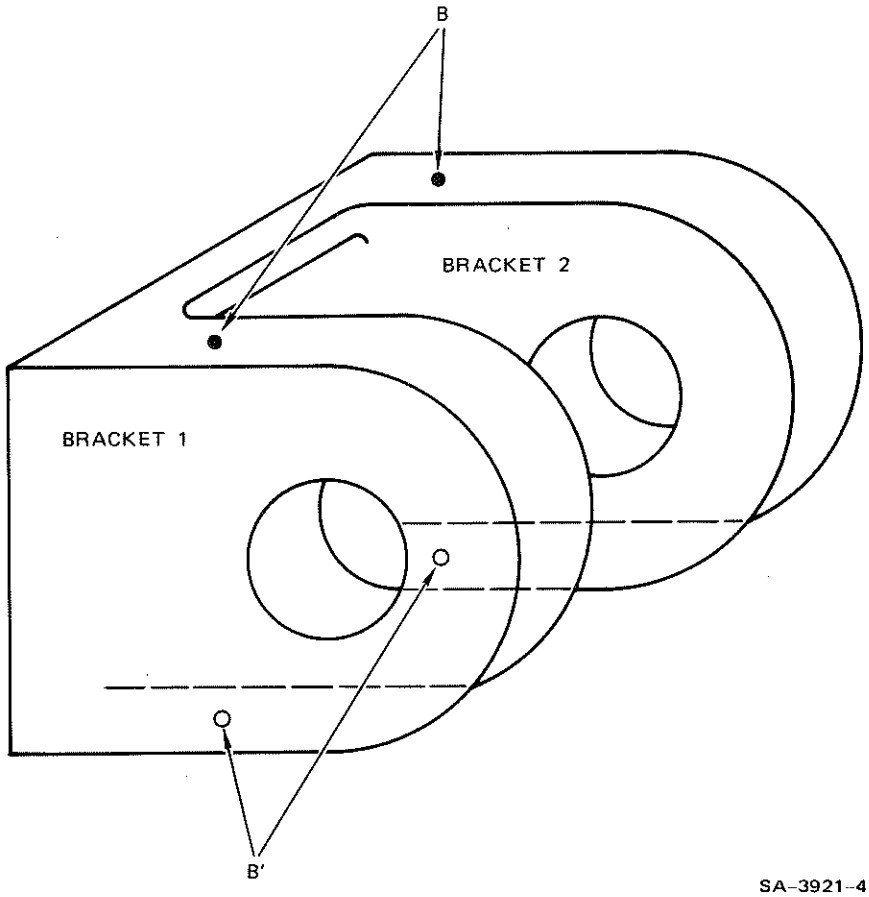

FIGURE IV-2 SUPPORT CASTING

equal sharing of the load, F_{ly} between the two support casting brackets. Even if this load is not equally shared between the brackets, the output voltage of the four-gage bridge should still be proportional to F_{ly}.

D. Construction Details

The strain gages and the electrical connections to them are delicate. To protect them from the elements, they were potted in Dow Corning RTV sealant. Protection from mechanical abuse, as well as electrical shielding, was provided by 0.25-inch thick steel covers. Despite these precautions, the strain gages are considered vulnerable. Because of the difficulty that would be encountered should one of the gages fail during the field tests, redundant sets of gages were installed.

Figure IV-3 is a photograph showing the strain gages mounted on one side of the lever arms. The protective covers have been removed to make the strain gages visible. Figure IV-4 is a photograph of the support casting. Again, the covers have been removed to show strain gages on one side.

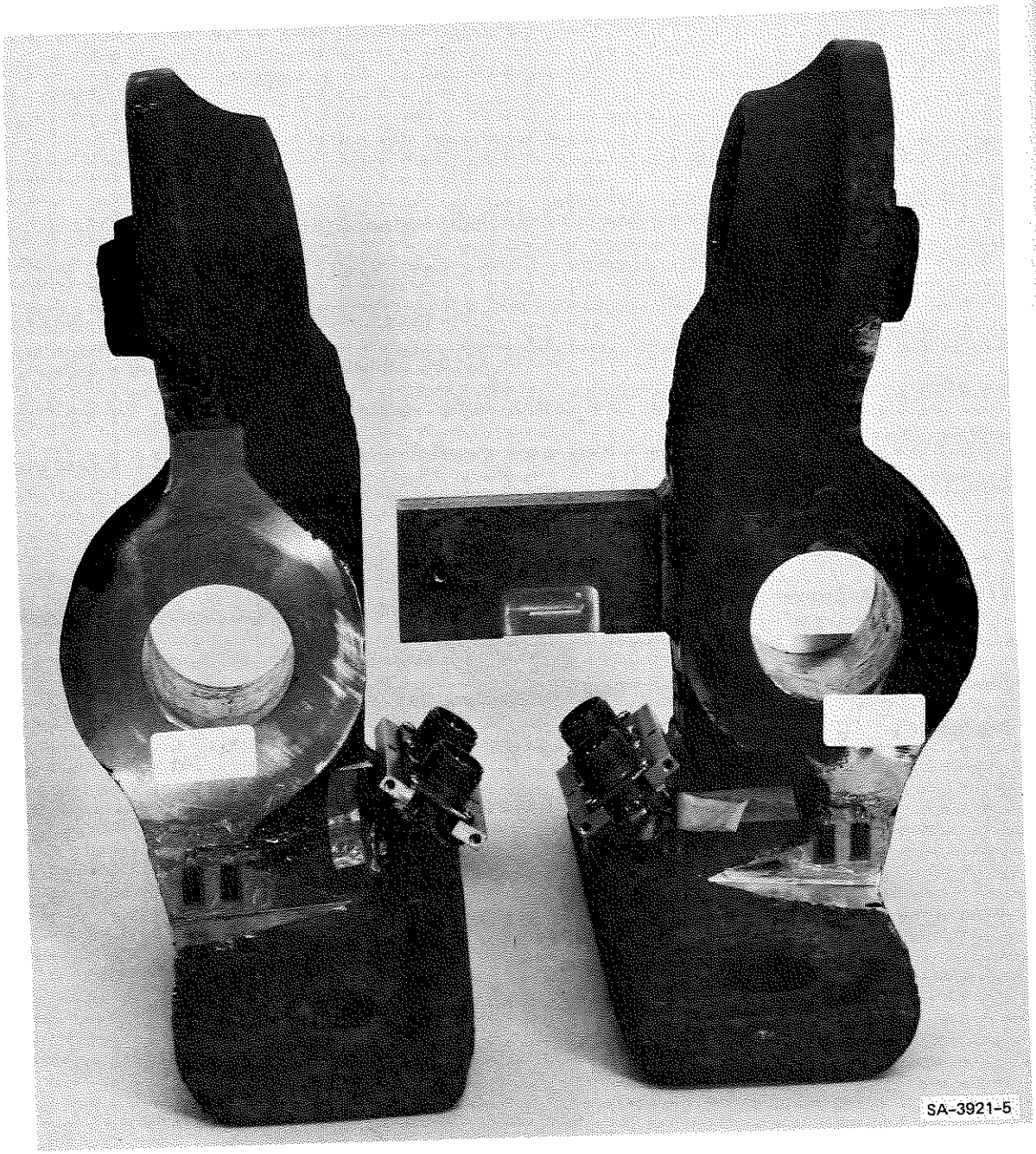

FIGURE IV-3 STRAIN GAGES ON LEVER ARMS

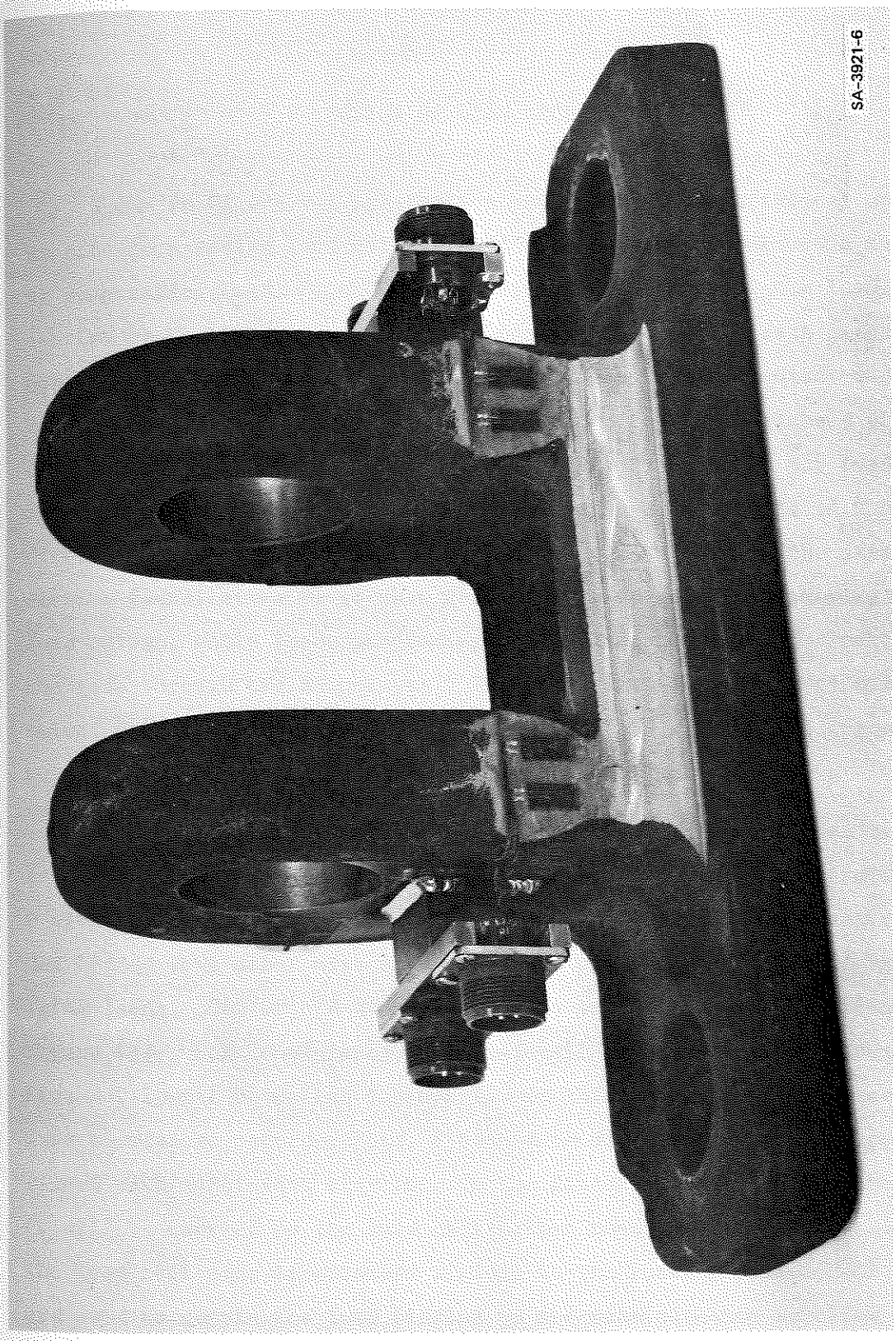

FIGURE IV-4 STRAIN GAGES ON SUPPORT CASTING

V DESIGN OF LOAD CELL MOUNTING

Shown in Figure V-1 are section and end views of a typical commercial tension-compression load cell. The device is used to measure a tension or compression load, P, at the load fitting. Nearly all the load, P, is carried by the load column which is instrumented with strain gages. The case protects the load column and strain gages from mechanical and chemical damage and also provides a rigid support for the periphery of the diaphragms. The purpose of the diaphragms is to transmit any loads other than P directly to the case. The diaphragms are very stiff in the radial direction (perpendicular to P), but are very compliant in the axial direction (parallel to P) so that the load, P, is carried primarily by the load column, while loads perpendicular to P are transmitted directly to the case through the diaphragms. The diaphragms are also very stiff in twisting so that any moments applied at the load fitting are transmitted to the case rather than carried by the load column.

A fundamental limitation of this type of load cell is that radial loads cannot exceed more than about 10 percent of the maximum value of P without damaging the load cell. To use the load cell to measure retarder loads, some means must be provided to protect the load cell from damaging loads. One of the simplest ways to accomplish this is shown in Figure V-2. For convenience, the load cell mounting concept shown in Figure V-2 will be called Concept I. In this concept, the load cell is used to measure retarder load, F (see Appendix A). The pivots are designed with sufficient clearance in the direction of F so that the load, F, will be carried by the load cell rather than by the support castings. The load cell case is attached rigidly to the running rail. Ball joints are used to couple the load fitting to the retarder shoe to allow for the motion of the shoe as wheels enter and leave the retarder.

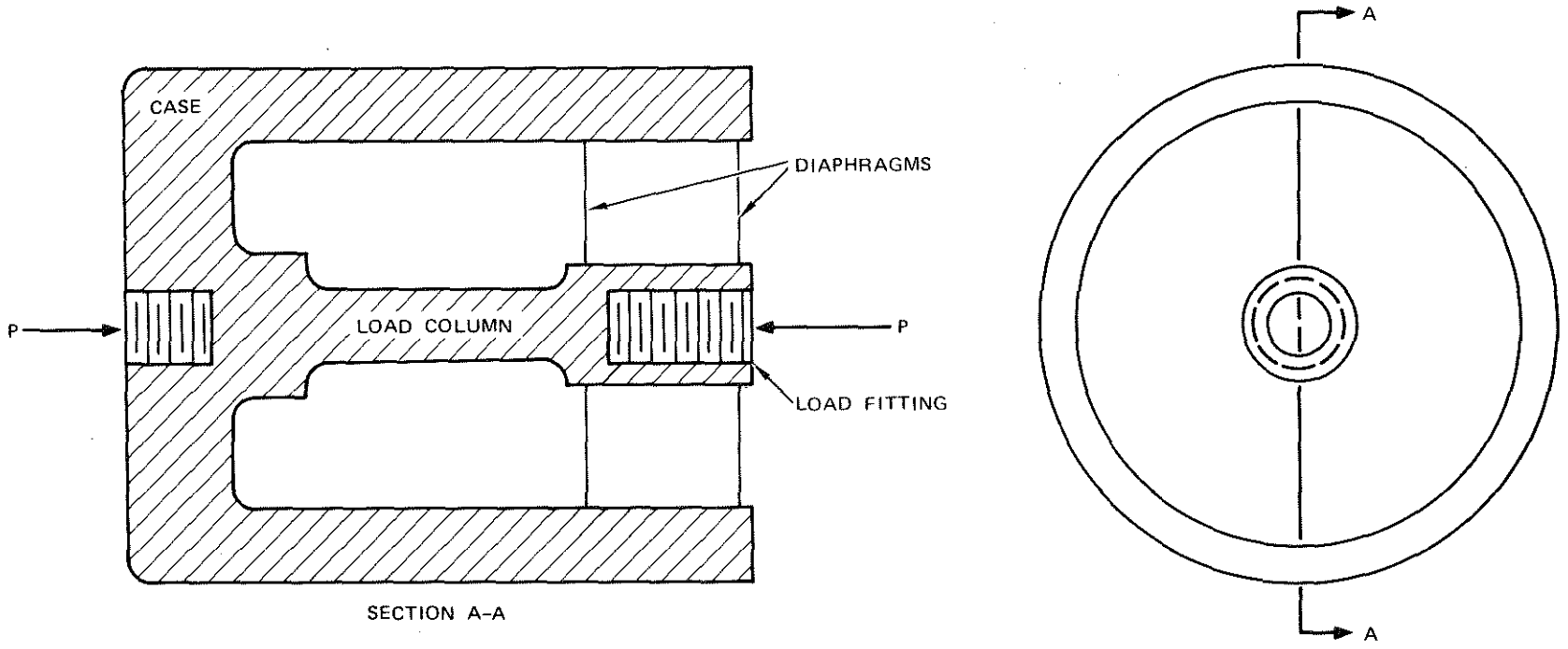

FIGURE V-1 TENSION-COMPRESSION LOAD CELL

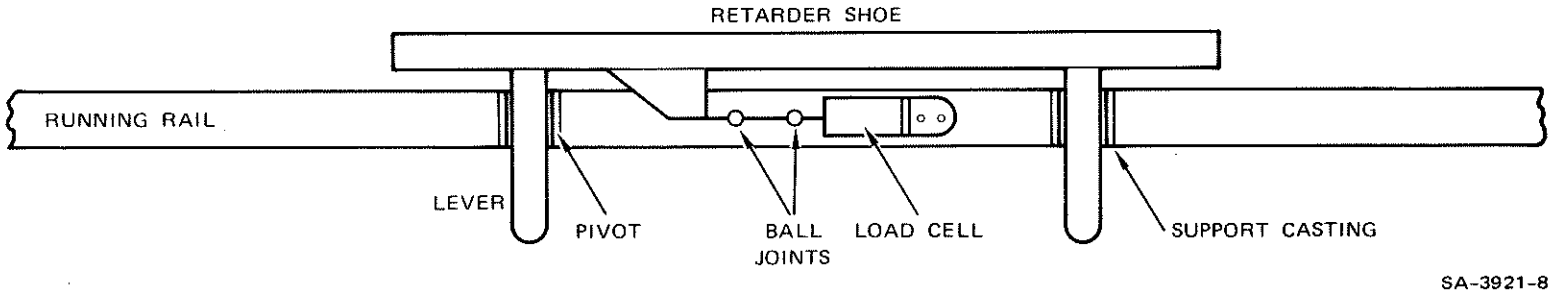

FIGURE V-2 CONCEPT I FOR LOAD CELL MOUNTING

If the friction at the pivots is too great, part or all of the load, F, will be transmitted to the running rail through the support castings rather than through the load cell. If this happens, the load cell output will not faithfully represent F and its value as an indicator of a slippery wheel will be diminished. This problem is particularly important in the case of the Abex retarder used in the tests because of the poor quality of the pivot bearing used in this retarder. The bearing consists of a rough steel pin which passes through a cast hole in the lever. Diametral clearance is approximately 0.13 inch. There is no provision for lubrication.

Because of the likelihood of problems with the friction of the pivot bearing in Concept I, a number of other load cell mounting concepts were generated. Figure V-3 shows one of these concepts, which will be called Concept II. In this design, the total retardation force, F_R, is measured by the load cell. A section of the running rail on which the retarder is mounted is severed from the main running rail, and is supported on linear bearings. A load cell is mounted to transmit x-direction forces from the severed section of the running rail to the main rail. High-quality linear bearings are available which exhibit sufficiently low friction so that F_R will be accurately measured by the load cell. How long such bearings would survive in the railroad yard environment, and how much maintenance they would require remain unanswered questions.

Concept II was representative of all subsequent concepts generated. The problem of high pivot friction leading to erroneous readings was avoided, but complexity and cost were greatly increased. The cost and complexity of slippery wheel detectors employing concepts such as Concept II would make them unattractive for widespread use in retarder yards. For this reason, the decision was made to mount the load cell as in Concept I.

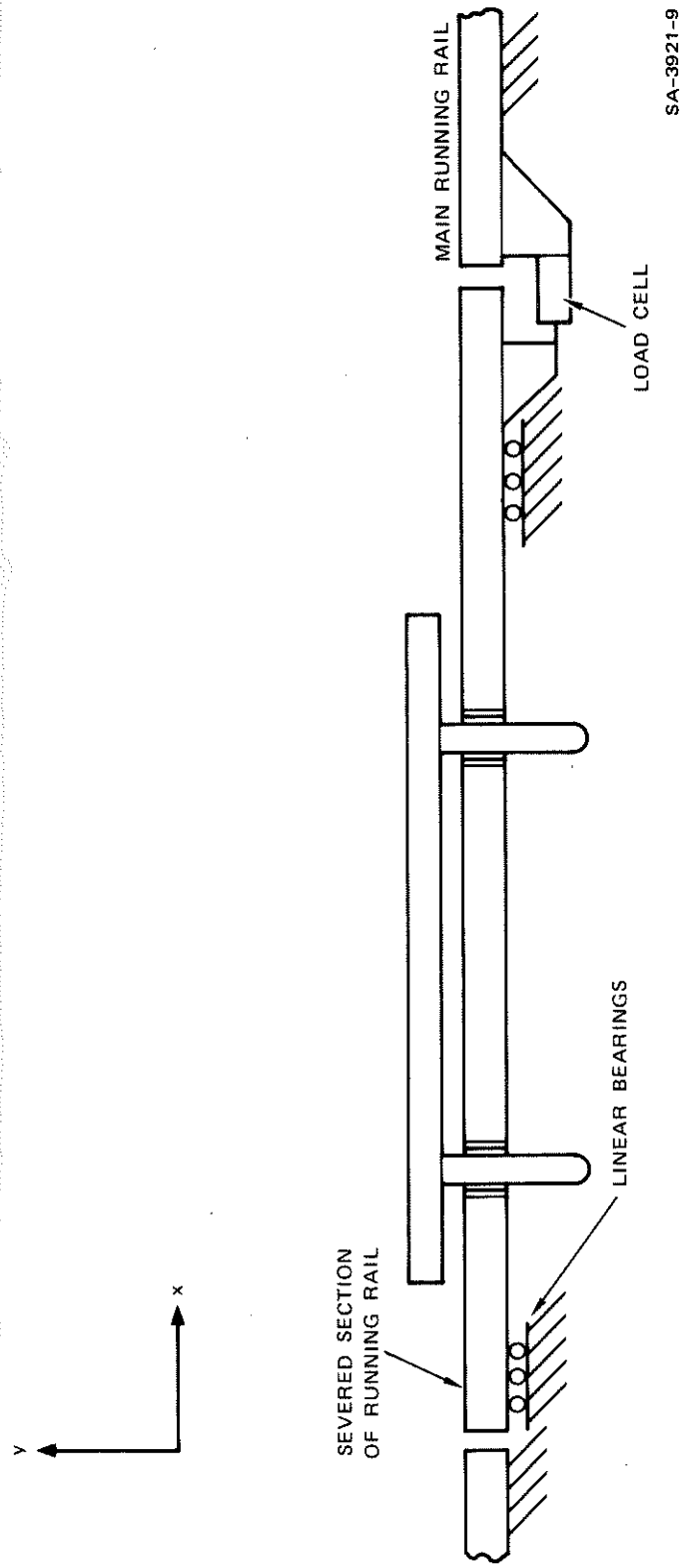

FIGURE V-3 CONCEPT II FOR LOAD CELL MOUNTING

To ameliorate problems with high pivot friction, the following improvements were made in the pivot:

(1) The pivot pin was replaced with a finely finished tool steel pin, hardened to Rockwell C60.

(2) The pivot bore in the lever was bored to a smooth finish.

(3) Diametral clearance between the pin and the bore was decreased to approximately 0.060 inch.

(4) The pivot pin was fitted with a grease fitting to permit lubrication of the pivot.

The load cell used was a BLH Electronics Model U3G2. Rated capacity of this unit was 20,000 pounds.

Figure V-4 is a photograph of the load cell mounted on the retarder.

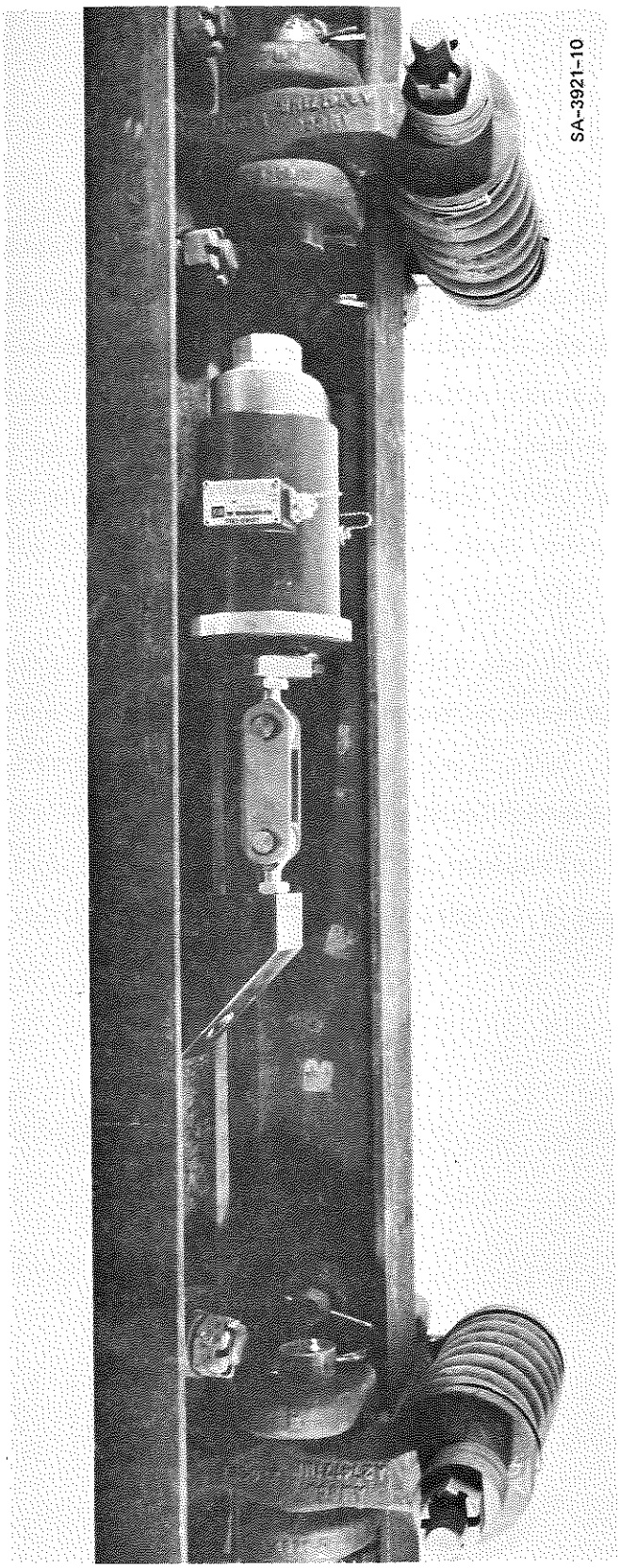

FIGURE V-4 LOAD CELL MOUNTED ON RETARDER

VI DESIGN OF ACCELEROMETER MOUNTING

Two mounting locations for the accelerometer were chosen, one on the retarder shoe, and one on lever 2. Each mounting location has provision for attachment of the accelerometer to measure x-, y-, or z-direction accelerations. The accelerometer mounting was easily changed so it would be possible to determine the optimum mounting position by trial and error when the field tests began. The mounting location chosen for the field tests was on the retarder shoe, measuring y-direction acceleration.

The charge amplifier used to amplify the accelerometer signal has a single-ended input. If the accelerometer were electrically connected to the retarder, a ground loop would result that could cause erroneous readings. To avoid this problem, the accelerometer is mounted with an insulated stud. There is no electrical connection between the accelerometer and the retarder so the ground loop is eliminated.

VII CALIBRATION: DESIGN CONSIDERATIONS

Shown in Figure VII-1 is the instrumented retarder, the retarder loads, F, M, and N, and transducer output voltages V_{A1}, V_{A2}, and V_B. The retarder loads are treated in detail in Appendix A. Combining Eqs. (15), (18), and (19), and (24) of Appendix A gives:

$$V_o = k_1 F \tag{1}$$

where k_1 is a constant, V_o is the output voltage from strain gages on the lever arm, and F is the longitudinal force exerted on the retarder shoe by the wheel. The analysis of Appendix A assumes that the stress in the retarder will be everywhere below the yield stress. With this assumption, the linearity of the elastic stress-strain equations implies that

$$V_o = k_2 M \text{ when } F = N = 0 \tag{2}$$

$$V_o = k_3 N \text{ when } F = M = 0 \tag{3}$$

where k_2 and k_3 are constants, M is the moment exerted on the retarder shoe by the wheel, and N is the normal force exerted on the shoe by the wheel. The analysis of Appendix A indicates that the constants k_2 and k_3 are zero, and this would indeed be true if the gages were perfectly aligned with the y-axis as has been assumed in Appendix A. In practice, the gages will never be perfectly aligned and the constants k_2 and k_3 will be small, but nonzero. The "super-position principle"[2] of mechanics allows us to combine Eqs. (1), (2), and (3) giving:

$$V_o = k_1 F + k_2 M + k_3 N \quad . \tag{4}$$

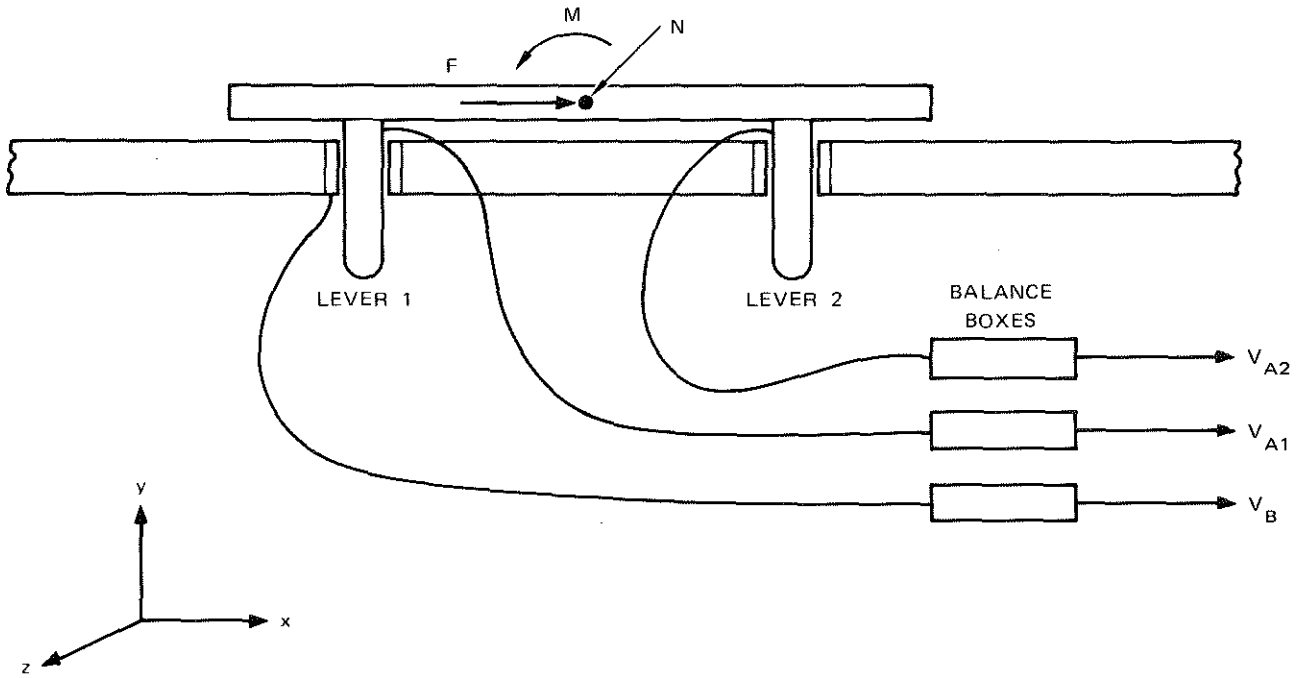

FIGURE VII-1 CALIBRATION PARAMETERS, RETARDER LOADS, AND TRANSDUCER OUTPUT VOLTAGES

An argument similar to the above can be made for the output voltage from strain gages on the support casting. The relations between the strain-gage bridge output voltages and the retarder loads are then given by

$$V_{A1} = k_{11}F + k_{12}M + k_{13}N \tag{5}$$

$$V_{A2} = k_{21}F + k_{22}M + k_{23}N \tag{6}$$

$$V_{B} = k_{31}F + k_{32}M + k_{33}N \tag{7}$$

where k_{11}, k_{12}, ... k_{33} are constants, V_{A1} is the output voltage from the strain-gage bridge on lever 1, V_{A2} is the voltage from the bridge on lever 2, and V_{B} is the voltage from the bridge on the support casting. The theoretical values of the constants k_{11} through k_{33} have been found using the equations of Appendix A and Appendix B:

$$k_{11} = \frac{V_i s_A c_A (G.F)}{2 I_A E} = 1.4 \times 10^{-5} \text{ volt/lb} \tag{8}$$

$$k_{12} = 0 \tag{9}$$

$$k_{13} = 0 \tag{10}$$

$$k_{21} = 0 \text{ or } k_{21} + k_{11} = \frac{V_i s_A c_A (G.F.)}{2 I_A E} \text{ (for large pivot friction)} \tag{11}$$

$$k_{22} = 0 \tag{12}$$

$$k_{23} = 0 \tag{13}$$

$$k_{31} = \frac{V_i s_B c_B (G.F.) b}{2 I_B E \ell} = 3.3 \times 10^{-7} \text{ volt/lb} \tag{14}$$

$$k_{32} = \frac{-V_i s_B c_B (G.F.)}{2 I_B E \ell} = -7.9 \times 10^{-8} \frac{\text{volt}}{\text{in-lb}} \tag{15}$$

$$k_{33} = 0 \tag{16}$$

Numerical values for these constants were calculated using $V_i = 5$ volts, G.F. = 118, and $E = 30 \times 10^6$ lb/in^2. Values of the other variables were taken from the Appendices.

Calibration is an alternate procedure for arriving at the above results. To calibrate the retarder, a known load, F, is applied to the retarder shoe and the values of V_{A1}, V_{A2}, and V_B are noted. From these data, k_{11}, k_{21}, and k_{31} can be calculated. The procedure is repeated with known loads M and N and the remaining k's are calculated from these data.

There are many reasons for performing this calibration procedure:

(1) Calibration verifies the proper functioning of the entire retarder/instrumentation system.

(2) Calibration serves as an independent check of the calculations that led to Eqs. (5) to (15).

(3) The results of tests on the instrumented retarder can be more readily interpreted if the values of the k's are known.

(4) While certain of the k's can be estimated from the above analysis, many of the k's can only be determined by calibration. [These are the k's that are zero in Eqs. (8) to (16).]

(5) The results of tests on the instrumented retarder will be more applicable to different retarder configurations in the future if the actual retarder loads are known. These loads can be calculated from the test results if the values of the k's are known.

For calibration, the load, N, was applied by a hydraulic cylinder placed between the two retarder shoes. A pressure gage was installed to monitor the hydraulic pressure. The force exerted by the cylinder is given by

$$f = pA \tag{17}$$

where F is the force, p is the pressure, and A is the cylinder area. The force, N, used for calibration was 22,000 pounds, which was the value of N expected in the field tests.

The load, F, was also applied with the cylinder. One end of the cylinder was supported by a fixture bolted to the running rail. The other end pushed on the end of the retarder shoe. The force, F, used for calibration was 600 pounds, which was the value of F expected in the field tests.

Shown in Figure VII-2 is the apparatus used to apply the moment, M, for calibration. Note that one retarder shoe has been removed from the retarder. Two jaws contact the remaining retarder shoe on opposite sides to apply the moment. The jaws are mounted on the end of a shaft that passes through ball bearings in the bearing support. The bearing support is attached to the running rail. An arm is attached to the shaft. The hydraulic jack pushes the arm upward, which causes a moment to be applied to the retarder shoe. The jaws are adjusted with shims so that as the arm is rotated, the jaws contact the retarder shoe simultaneously. This ensures that when the moment is applied, a force is not also applied. The moment, M, used for calibration was 10,000 in-lb, which was the value of N expected in the field tests.

FIGURE VII-2 APPARATUS FOR MOMENT CALIBRATION

VIII CALIBRATION RESULTS

Data from retarder calibration are tabulated in Table VIII-1. The redundant pairs of strain-gage bridges have been identified as "primary" and "secondary." Data for these bridges are tabulated in Tables VIII-1 and VIII-2, respectively.

When calibration was performed, we found that friction at the pivots was significant. This is reflected in the calibration data in two ways:

(1) To get repeatable results, it was necessary to combine the outputs of strain-gage bridges on the two lever arms when measuring the response to a longitudinal force, F. This problem is discussed in Sections IV and V, "Design of Strain Gage Mounting," and "Design of Load Cell Mounting," respectively.

(2) The pivot friction also caused some scatter in a number of other measurements. For these cases, the average value of a number of measurements is entered in Tables VIII-1 and VIII-2 and the standard deviation from this average, σ, expressed as a percentage is entered. For measurements with deviations of less than 5 percent, no deviation value is entered.

The constants k_{11}, k_{12}, ... k_{33} were calculated from calibration data. These values are tabulated in Tables VIII-3 and VIII-4 together with the theoretical values for comparison. (The theoretical values are derived in Section VII, "Calibration: Design Considerations.")

The calibration results for V_{A1} and V_{A2} are best understood by considering their sum, $V_{A1} + V_{A2}$. As noted above, this is necessary due to the significant pivot friction. Combining Eqs. (5) and (6) of Section VII gives

Table VIII-1

CALIBRATION DATA FOR PRIMARY BRIDGES

Bridge Output Voltages $V_{final} - V_{initial}$	Test Conditions		
	M = 0 N = 22,000 lb $F_{initial}$ = 0 F_{final} = 600 lb	F = 0 N = 22,000 lb $M_{initial}$ = 0 M_{final} = -10,000 in-lb	F = 0 M = 0 $N_{initial}$ = 0 N_{final} = 22,000 lb
V_{A1}	+3.1 mV* σ = 17%	+2.8 mV	-26 mV
V_{A2}	+3.1 mV* σ = 17%	-3.1 mV	-13 mV
V_B	-0.40 mV σ = 10%	+0.20 mV	-25 mV

*Figure reported is ($V_{A1} = V_{A2}$).

Table VIII-2

CALIBRATION DATA FOR SECONDARY BRIDGES

Bridge Output Voltages $V_{final} - V_{initial}$	Test Conditions		
	M = 0 N = 22,000 lb $F_{initial}$ = 0 F_{final} = 600 lb	F = 0 N = 22,000 lb $M_{initial}$ = 0 M_{final} = -10,000 in-lb	F = 0 M = 0 $N_{initial}$ = 0 N_{final} = 22,000 lb
V_{A1}	+2.6 mV σ = 9%	+2.6 mV	-31 mV
V_{A2}	+2.6 mV* σ = 9%	-4.0 mV	+10 mV
V_B	+0.47 mV σ = 26%	+0.22 mV	-15 mV

*Figure reported is $(V_{A1} + V_{A2})$.

Table VIII-3

THEORETICAL AND EXPERIMENTAL
VALUES OF k FOR PRIMARY BRIDGES

Constant	Theoretical	Calculated from Calibration Data
k_{11}	$1.4 \times 10^{-5} \frac{volt^*}{lb}$	$5.2 \times 10^{-6} \frac{volt^*}{lb}$
k_{12}	0	$-2.8 \times 10^{-7} \frac{volt}{in\text{-}lb}$
k_{13}	0	$1.2 \times 10^{-6} \frac{volt}{lb}$
k_{21}	$1.4 \times 10^{-5} \frac{volt^*}{lb}$	$5.2 \times 10^{-6} \frac{volt^*}{lb}$
k_{22}	0	$3.1 \times 10^{-7} \frac{volt}{in\text{-}lb}$
k_{23}	0	$-5.9 \times 10^{-7} \frac{volt}{lb}$
k_{31}	$3.3 \times 10^{-7} \frac{volt}{lb}$	$-6.7 \times 10^{-7} \frac{volt}{lb}$
k_{32}	$-7.9 \times 10^{-8} \frac{volt}{in\text{-}lb}$	$-2.0 \times 10^{-8} \frac{volt}{in\text{-}lb}$
k_{33}	0	$-1.1 \times 10^{-6} \frac{volt}{lb}$

*Value entered is $k_{11} + k_{21}$.

Table VIII-4

THEORETICAL AND EXPERIMENTAL
VALUES OF k FOR SECONDARY BRIDGES

Constant	Theoretical	Calculated from Calibration Data
k_{11}	$1.4 \times 10^{-5} \frac{\text{volt}^*}{\text{lb}}$	$4.3 \times 10^{-6} \frac{\text{volt}^*}{\text{lb}}$
k_{12}	0	$-2.6 \times 10^{-6} \frac{\text{volt}}{\text{in-lb}}$
k_{13}	0	$-1.4 \times 10^{-6} \frac{\text{volt}}{\text{lb}}$
k_{21}	$1.4 \times 10^{-5} \frac{\text{volt}^*}{\text{lb}}$	$4.3 \times 10^{-6} \frac{\text{volt}^*}{\text{lb}}$
k_{22}	0	$4.0 \times 10^{-7} \frac{\text{volt}}{\text{in-lb}}$
k_{23}	0	$4.5 \times 10^{-7} \frac{\text{volt}}{\text{lb}}$
k_{31}	$3.3 \times 10^{-7} \frac{\text{volt}}{\text{lb}}$	$7.8 \times 10^{-7} \frac{\text{volt}}{\text{lb}}$
k_{32}	$-7.9 \times 10^{-8} \frac{\text{volt}}{\text{in-lb}}$	$-2.2 \times 10^{-8} \frac{\text{volt}}{\text{in-lb}}$
k_{33}	0	$-6.8 \times 10^{-7} \frac{\text{volt}}{\text{lb}}$

*Value entered is $k_{11} + k_{21}$.

$$V_{A1} + V_{A2} = (k_{11} + k_{21})F + (k_{12} + k_{22})M + (k_{13} + k_{23})N \quad . \qquad (1)$$

Using the experimental values from Table VIII-3, Eq. (1) becomes

$$V_{A1} + V_{A2} = (5.2 \times 10^{-6} \frac{\text{volt}}{\text{lb}})F + (3.0 \times 10^{-8} \frac{\text{volt}}{\text{in-lb}})M$$

$$+ (6.1 \times 10^{-7} \frac{\text{volt}}{\text{lb}})N \quad . \qquad (2)$$

For the retarder to be an effective slippery wheel detector, one should be able to calculate F if $V_{A1} + V_{A2}$ is known. Referring to Eqs. (1) and (2), this would be more easily done if the coefficient $k_{12} + k_{22}$ were zero. Referring to Tables VIII-3 and VIII-4, k_{12} and k_{22} have opposite signs, but the magnitude of k_{22} is greater. The moment, M, used for determining k_{12} and k_{22} was applied at a point on the retarder shoe closer to lever 2 than to lever 1. the situation is difficult to treat analytically, but application of St. Venant's Principle[3] indicates that if the point of application of the torque, M moved toward the center of the retarder shoe, k_{12} would increase in absolute magnitude and k_{22} would decrease. Eventually, a point would be reached (somewhere near the center of the retarder) where k_{12} and k_{22} would have exactly equal magnitude and opposite signs. If the above conjectures prove to be true, then when the wheel is near the center of the retarder shoe, Eq. (2) becomes

$$V_{A1} + V_{A2} = (5.2 \times 10^{-6} \frac{\text{volt}}{\text{lb}})F + (6.1 \times 10^{-7} \frac{\text{volt}}{\text{lb}})N \quad . \qquad (3)$$

Now, if N remains constant, F can be calculated directly from $V_{A1} + V_{A2}$. The value of F calculated in Appendix A is 600 pounds. If we assume a typical value for F is 600 pounds and the nominal normal force, N, is 22,000 pounds, then N can vary as much as 1.2 percent and the resulting error in F calculated from $V_{A1} + V_{A2}$ will be less than 10 percent.

Normal force of the experimental retarder depends only on the wheel width and the thickness of retarder shoes. For the purposes of our tests with the experimental retarder, the variation of N should not be a problem since the wheel width will be known and the wear of retarder shoes should be negligible.

A variation of N of less than 1 percent could probably be achieved in a slippery wheel detector designed for continual service by substituting hydraulic cylinders for the springs being used on the experimental retarder. When this is done, N is independent of wheel width or shoe thickness.

Using the values of Table VIII-3 in Eq. (7) of Section VII gives

$$V_B = (-6.7 \times 10^{-7} \frac{\text{volt}}{\text{lb}})F - (2.0 \times 10^{-8} \frac{\text{volt}}{\text{in-lb}})M - (1.1 \times 10^{-6} \frac{\text{volt}}{\text{lb}})N \quad . \qquad (4)$$

The value of M calculated in Appendix A is -10,000 in-lb. Using this value for M, it can be shown that in order for M to be calculated from V_B with 10 percent accuracy, the normal force, N, must be known to within ±0.08 percent. Measurement of N to this accuracy would be very difficult. It would also be difficult to control N this precisely with a hydraulic cylinder, as suggested above. For these reasons, it seems unlikely that V_B will be useful for slippery wheel detection.

IX DESIGN OF INSTRUMENTATION

During the retarder tests, transducer outputs were recorded on an Ampex FR-1300A seven-channel tape recorder. The recorder also has a voice channel, which was used to identify the tests. The instrumentation system must amplify the transducer output signals to a 1-volt peak level for the tape recorder.

Table IX-1 lists the function of each recorder channel together with specifications for the associated instrumentation. The gain for channels 1, 2, 3, and 4 was found by assuming the maximum friction coefficient, μ, would be 0.6. The equations of Appendices A and B were then used to find the necessary gain for a 1-volt output to correspond to the loads generated when $\mu = 0.6$. A friction coefficient of 0.1 to 0.2 is expected for normal (not slippery) wheels. The value of $\mu = 0.6$ has been used in the gain computation to ensure against the possibility of saturating the tape recorder with any abnormally large signals. It was also assumed that the minimum value of μ, corresponding to a slippery wheel, would be 0.01. The maximum input noise was chosen to be 10 percent of the signal expected when μ is 0.01. Previous tests[4] indicate that 250 g is the maximum acceleration to be expected at the accelerometer. This value was assumed to calculate the gain for channel 5. For channels 1, 2, 3, and 4, a power source for transducer excitation must be included.

Figure IX-1 is a block diagram of the instrumentation and its connection to transducers and recorder.

The transducers for channels 1, 2, 3, and 4 are each strain gage bridges. Figure IX-2 is a schematic of such a bridge. The transducer for channel 1 is contained in the load cell. For channels 2, 3, and 4,

Table IX-1

INSTRUMENTATION SPECIFICATIONS

Characteristic	Channel Number					
	1	2	3	4	5	6
Function	Load Cell	Lever 1, strain gage A	Lever 2, strain gage A	Strain gage B	Accelerometer	Push button
Minimum bandwidth	1 kHz	1 kHz	1 kHz	1 kHz	10 kHz	10 Hz
Gain	300	15	20	180	340 V/μC	1
Maximum input noise	5 μV	50 μV	50 μV	10 μV	50 pC	n.a.
Minimum input impedance	100 kΩ	100 kΩ	100 kΩ	100 kΩ	10 MΩ	n.a.
Excitation	5 V	5 V	5 V	5 V	n.a.	1 V

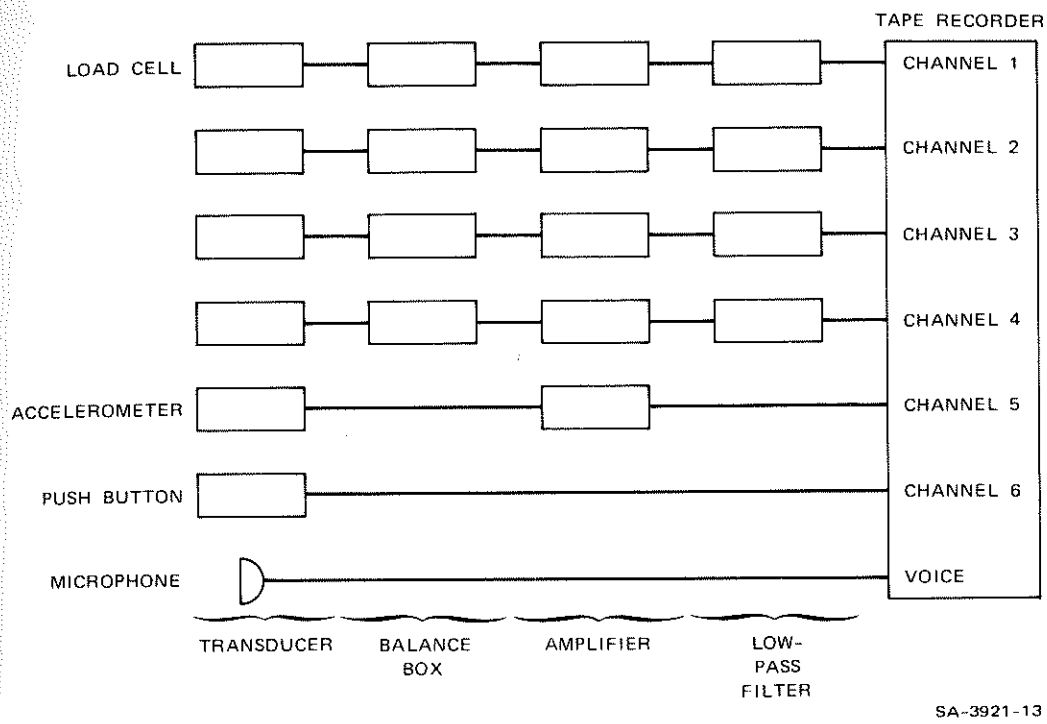

FIGURE IX-1 TRANSDUCERS, INSTRUMENTATION, AND RECORDER, BLOCK DIAGRAM

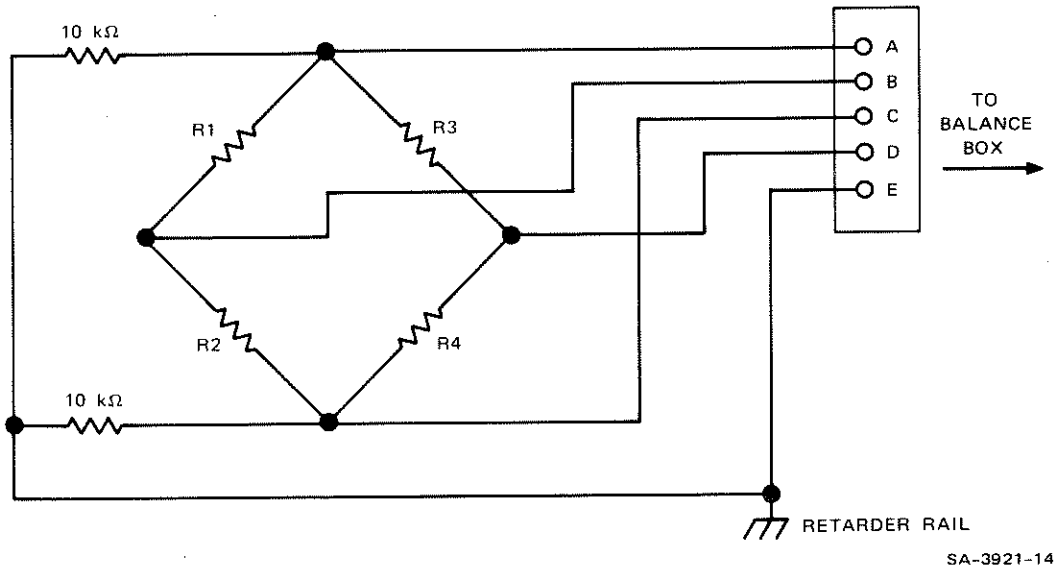

FIGURE IX-2 TRANSDUCER, SCHEMATIC DIAGRAM

the transducers are composed of strain gages mounted on the retarder and of 350-ohm fixed resistors as follows:

Table IX-2

STRAIN GAGE LOCATIONS

Channel	R1	R2	R3	R4
2	Fixed resistor	Fixed resistor	Gage A, lever 1	Gage A′, lever 1
3	Fixed resistor	Fixed resistor	Gage A, lever 2	Gage A′, lever 2
4	Gage B′, bracket 2	Gage B, bracket 2	Gage B, bracket 1	Gage B′, bracket 1

The transducer for channel 5 is an Endevco Model 2221C piezoelectric accelerometer.

The "transducer" for channel 6 is a push-button switch. This switch was operated by an assistant to indicate when the wheels passed the center of the retarder.

Figure IX-3 is a simplified schematic diagram of a balance box. This device has two functions:

- To provide excitation power for the transducer. This power is supplied by the battery. The 1.5 K-ohm potentiometer is used to adjust the excitation to 5 volts.
- To provide adjustable compensation for initial bridge in-balance. This is accomplished with the 10K-ohm potentiometer and associated fixed resistor.

The amplifier for channels 1, 2, 3, and 4 is a Hewlett-Packard Model 2470A Data Amplifier. The amplifier for channel 5 is a Kistler Model 568 Charge Amplifier.

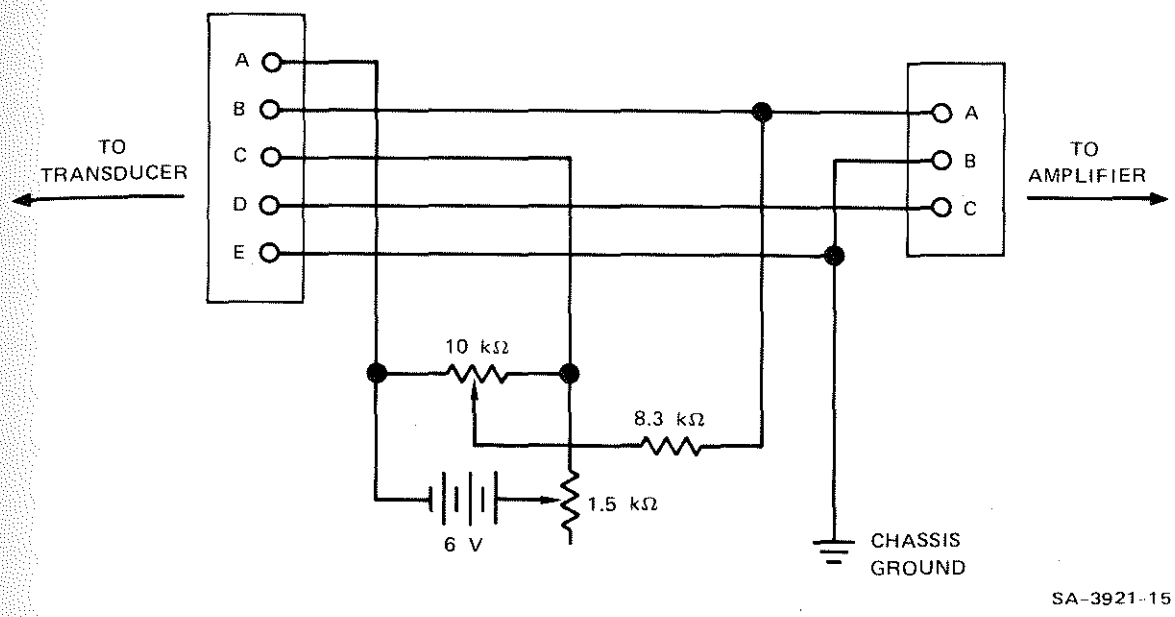

FIGURE IX-3 BALANCE BOX, SIMPLIFIED SCHEMATIC DIAGRAM

Pickup of undesired signals--most often radiation from 60-Hz power lines--is often a problem with a high-gain instrumentation system such as this one. Careful grounding and shielding will usually minimize the problems.[5] Figure IX-4 is a simplified schematic diagram of a typical instrumentation channel showing the grounding and shielding used. The transducer and excitation source are shielded and grounded at the retarder rail. The tape recorder is grounded at the ac power ground. Any voltage difference between the two grounds will appear as a common-mode input to the amplifier and will be rejected.

Another form of noise that was anticipated was high-frequency vibration of the retarder, which would be picked up by the strain gages and load cell. In principle, this noise could be filtered when the tape was played back. However, preliminary tests indicated that the amplitude of the vibrations would be great enough to saturate the tape recorder, which would result in loss of the desired, low-frequency data. To solve this

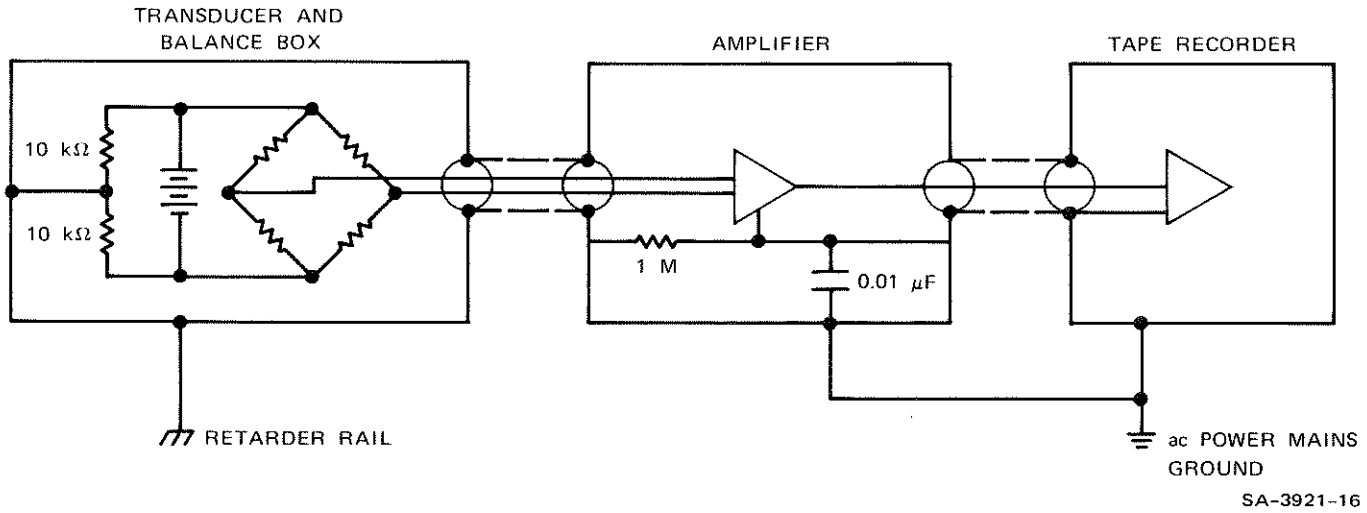

FIGURE IX-4 GROUNDING AND SHIELDING, SIMPLIFIED SCHEMATIC DIAGRAM

problem, low-pass filters, shown in Figure IX-1 were used ahead of the tape recorder. A schematic diagram for one of the filters is shown in Figure IX-5. The corner frequency for this filter is about 10 Hz.

Figure IX-6 is a photograph of the instrumentation, which was set up in the rear of a van at the field test site. At the bottom right is the tape recorder on which the instrumentation signals were recorded. Above the tape recorder is an oscilloscope, which was used to monitor the recorded signals. On the left is a rack containing the remainder of the instrumentation. On top are the four balance boxes. Below these are the charge amplifier on the left and the low-pass filters on the right. Below these are the four amplifiers for the load cell and strain gage signals.

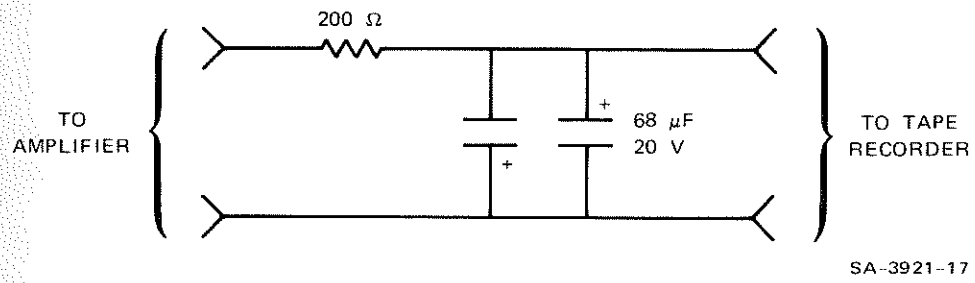

FIGURE IX-5 LOW-PASS FILTER

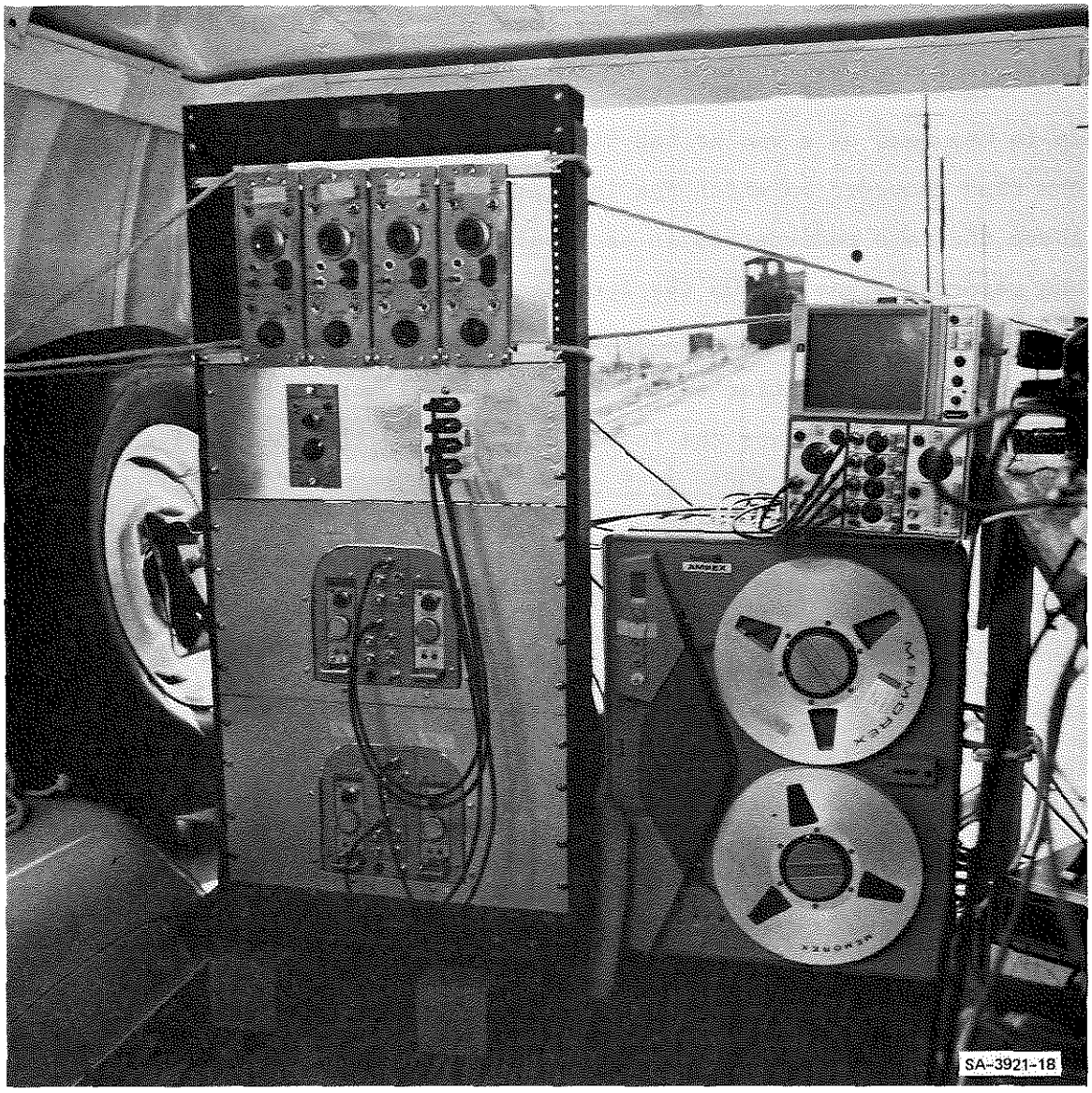

FIGURE IX-6 INSTRUMENTATION AT FIELD SITE

X FIELD TESTS

Field tests of the instrumented retarder were conducted at the Richmond Yard of the Southern Pacific Transportation Company on 19 May 1975 and on 27 May 1975.

On 19 May, retarder instrumentation signals were recorded for a number of cars that passed through the retarder as part of the normal yard operations. The purpose of these tests was to verify proper functioning of the retarder and instrumentation system.

On 27 May, six selected cars were used for testing. The cars were selected to represent typical rolling stock encountered in normal yard operations. Characteristics of these cars are tabulated in Table X-1.

Testing consisted of 12 "runs" as follows:

(1) Push all six cars through the retarder.

(2) Push all six cars through the retarder.

(3) Push all six cars through the retarder.

(4) Coat retarder and wheel rims of first car with SAE 30 oil and push all six cars through retarder.

(5) Coat retarder and wheel rims of first car with SAE 30 oil and push all six cars through retarder.

(6) Push all six cars through the retarder.

(7) Coat retarder and wheel rims of all cars with SAE 30 oil and push cars through retarder.

(8) Push all six cars through the retarder.

(9) Push all six cars through the retarder.

(10) Coat retarder and wheel rims of all cars with Moluballoy 882 EP O.G. heavy grease. Push all cars through the retarder.

(11) Push all six cars through the retarder.

(12) Push all six cars through the retarder.

Table X-1

CHARACTERISTICS OF TEST CARS

Characteristic	Car Sequence Number					
	1	2	3	4	5	6
Initials and number	EFCS 3914	SP 245435	SP 242441	SP 243069	GN 37364	MILW 50336
Date built	March 72	September 74	September 72	March 73	August 63	November 74
Type	70-T box	70-T box	70-T box	70-T box	70-T box	70-T box
Weight	151,960	145,620	144,980	145,220	62,700	59,200
Type wheels	MW*	SW†	SW	SW	SW	SW

*MW = multiple wear.

†SW = single wear.

Retarder instrumentation signals were recorded as the cars passed through the instrumented retarder. After each run, the cars were each released at the hump; retardation in a conventional (not instrumented) retarder was measured by Southern Pacific personnel using a Doppler radar. The conventional retarder was lubricated in the same manner as the instrumented retarder before runs 4, 5, 7, and 10.

The weather on 27 May was clear; the average temperature was approximately 85°F.

Figure X-1 is a photograph taken during the field tests. In the foreground is the instrumented retarder that is being coated with grease. In the background, on the left, is the van in which the instrumentation is mounted.

FIGURE X-1 GREASING THE INSTRUMENTED RETARDER SHOES

XI TEST RESULTS AND DISCUSSION

A. Introduction

A primary purpose of the retarder field tests is to determine which, if any, of the instrumentation signals can be used to indicate a slippery wheel. If a number of signals can be used, we would like to know which is the "best" indicator of slippery wheels, and how "good" it is. To facilitate comparison of the different instrumentation signals, the same general scheme of data reduction has been used for each.

The first step in the data reduction is to determine an algorithm that will, given the time-dependent signal for one wheel, assign a number to that wheel that is correlated with wheel "slipperiness." This parameter will be called the "retardation index." The choice of algorithm is influenced by the theoretical models of retarder operation presented in previous sections, as well as by the characteristics of the recorded signal. The algorithms chosen for each signal are believed to be nearly optimal, but there is no way of knowing if the "best" algorithm has been chosen.

The second step in the data reduction is to compare the retardation index to the retardation measured for each car in the conventional retarder. To make this comparison possible, the retardation indices of the wheels of a given car are averaged and the result is the retardation index for that car. Listed in Table XI-1 are the retardations measured in the conventional retarder, F_r. The retardation index for each car on each run is plotted against the measured retardation of that car. Figure XI-1 is an example of such a plot, known as a "scattergram." In this figure, measured retardation is plotted on the horizontal axis and the

Table XI-1

RETARDATION IN CONVENTIONAL RETARDER
(Ft-lb per Lineal Foot of Retarder)

Run	Car					
	1	2	3	4	5	6
1	8,880	7,050	9,550	9,620	7,420	7,820
2	9,600	6,760	9,650	9,630	5,870	8,550
3	10,100	7,950	10,200	10,400	6,280	8,970
4	3,530	3,130	5,290	8,000	5,220	8,030
5	4,770	2,330	3,330	4,250	4,440	5,580
6	5,340	2,690	2,650	3,360	3,260	4,560
7	3,140	2,250	3,040	3,560	1,890	3,890
8	3,140	2,400	2,840	3,850	1,960	3,720
9	2,950	2,110	3,040	3,560	2,090	3,460
10	3,430	2,040	3,720	3,260	1,960	3,970
11	2,570	2,040	3,230	3,160	1,500	3,800
12	2,100	2,040	3,430	3,160	1,500	3,550

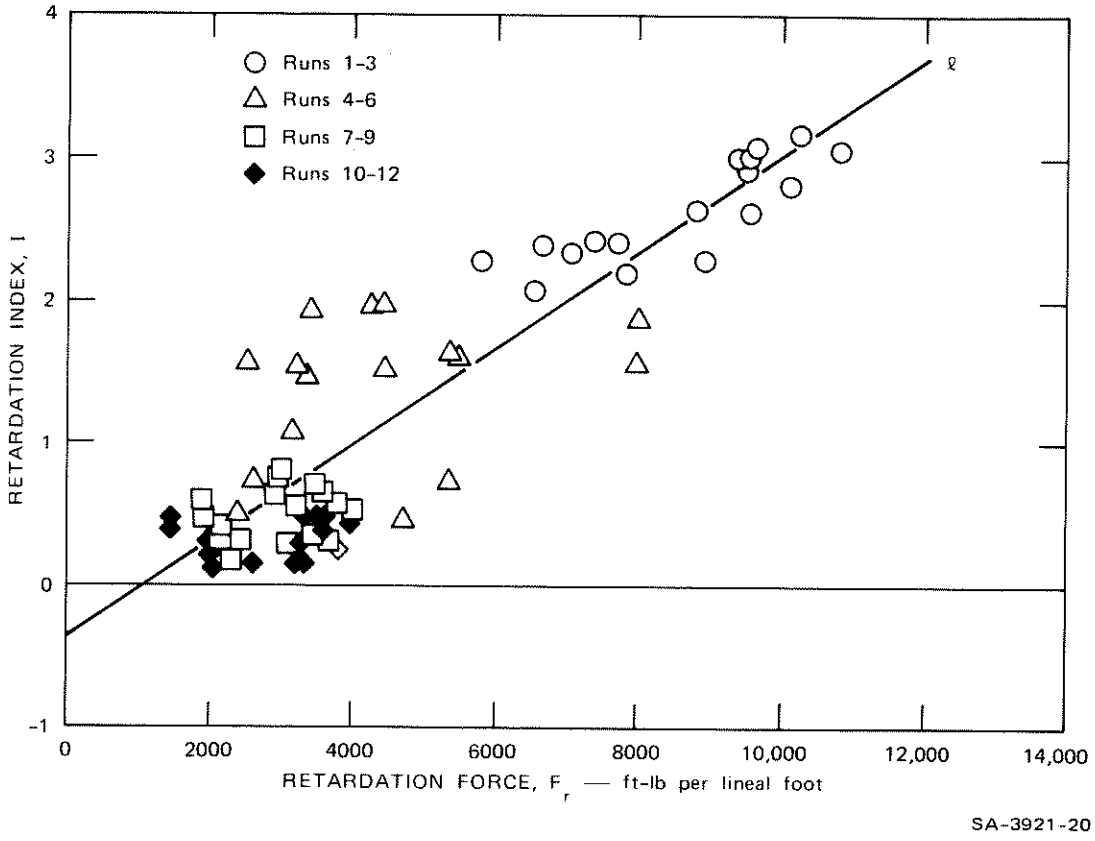

FIGURE XI-1 SCATTERGRAM FOR LOAD CELL SIGNAL

retardation index derived from the load cell signal (described below in Section B) is plotted on the vertical axis. Since there were 12 test runs and six cars in each run, one would expect each scattergram to contain 72 points. In fact, the number of points is always less than 72. This is because certain points are deleted from the plot and all subsequent analyses, either because of equipment malfunction or because the car stopped with a wheel in the instrumented retarder.

Inspection of the scattergram quickly reveals the relationship between the retardation index and the measured retardation. A small amount of "scatter" (points nearly all on a single, straight line) is indicative of a signal that could be a "good" indicator of a slippery wheel.

The third step in the data reduction is a statistical analysis, which yields an estimate of the percentage of "false alarms" to be expected if the signal were used for slippery wheel detection in active classification yards. Inspection of a scattergram can give an intuitive feeling for the characteristics of a signal, and one might even choose a signal for slippery wheel detection on the basis of this plot alone. However, it could be difficult to determine, from inspection of two scattergrams, which represented the "better" signal for slippery wheel detection. It would be even more difficult to say <u>how much</u> better one signal was. The statistical analysis allows us to address these questions in a more rational manner, and to find quantitative answers. The statistical analysis is described briefly below in Section D. The mathematical details are contained in Appendix C.

B. <u>Load Cell Signal</u>

Shown in Figure XI-2 is a typical load cell signal. The signal shown is for one truck (two axles). Also shown in the figure are times t_1, t_2, t_3, t_4, and t_5, which correspond to positions of the wheel in

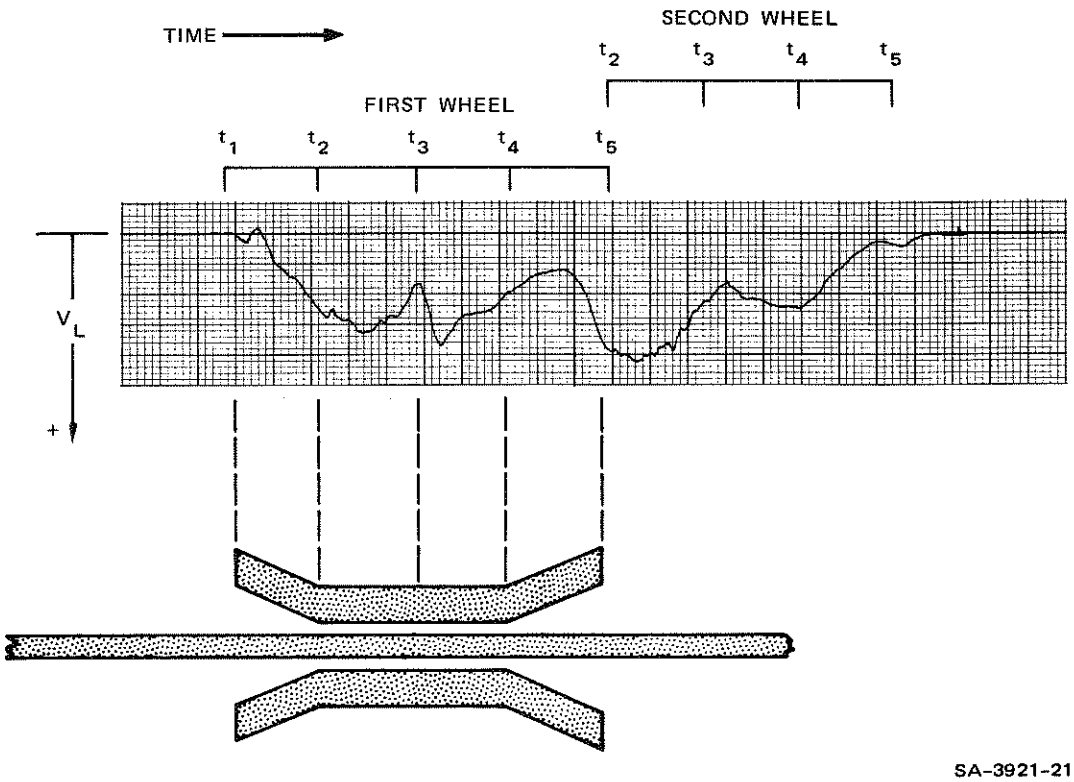

FIGURE XI-2 TYPICAL LOAD CELL SIGNAL FOR ONE TRUCK

the retarder shown in the figure and described below:

- (t_1) Wheel first contacts retarder shoe
- (t_2) Wheel enters straight section of retarder shoe
- (t_3) Wheel in center of retarder
- (t_4) Wheel leaves straight section of retarder
- (t_5) Wheel leaves retarder.

In a slippery wheel detector for use in an active classification yard, wheel-operated switches would probably be used to provide signals at t_2, t_3, and t_4. During the field tests, an assistant manually closed a switch at t_3. From the switch signal at t_3, t_2, and t_4 were found by

considering the retarder and truck geometry and the car velocity. In particular, if the time between t_3 for the two axles of a truck is t_x (see Figure XI-2), then

$$t_4 \cong t_3 + \frac{t_x}{3}$$
$$t_2 \cong t_3 - \frac{t_x}{3} \qquad (1)$$

Between t_1 and t_2, the wheel is entering the retarder. During this time, the retarder load, F, increases as the normal force, N, rises. The load cell measures F so its output also rises. At t_2, the wheel is opposite a lever arm and the normal force, N, is at a maximum as is F and the load cell signal. At t_3, the wheel is between two lever arms. Because of deformation of the retarder shoes, N is smaller than at t_2 and as a result, F and the load cell signal are decreased from the maximum at t_2. The load cell signal reaches a second maximum at t_4, opposite the second lever arm, and decreases to zero at t_5 as the wheel leaves the retarder.

Let V_L be the load cell signal voltage recorded in the field tests. The algorithm chosen for finding the retardation index, I, for the load cell signal was

$$I = \frac{(4 \text{ volt}^{-1})}{t_4 - t_2} \int_{t_2}^{t_4} V_L \, dt \quad . \qquad (2)$$

Thus, I is a measure of the average value of F between t_2 and t_4. The constant, 4 volt^{-1}, was chosen for convenience and to give numerical values of I similar to those for the other signals below.

The scattergram for the load cell signal is shown in Figure XI-1. Also shown in this figure is the line, ℓ, discussed in Appendix C. On the basis of this plot alone, it is clear that there is a strong correlation between the retardation index and measured retardation. The statistical analysis indicates that if the load cell signal were used for a slippery wheel detector, the probability of false alarms would be about 0.84 percent.

C. Strain Gages on the Lever Arms

Typical recorded signals from the strain gages on the lever arms (V_{A1} and V_{A2}) are shown in Figure XI-3 together with their sum. It has

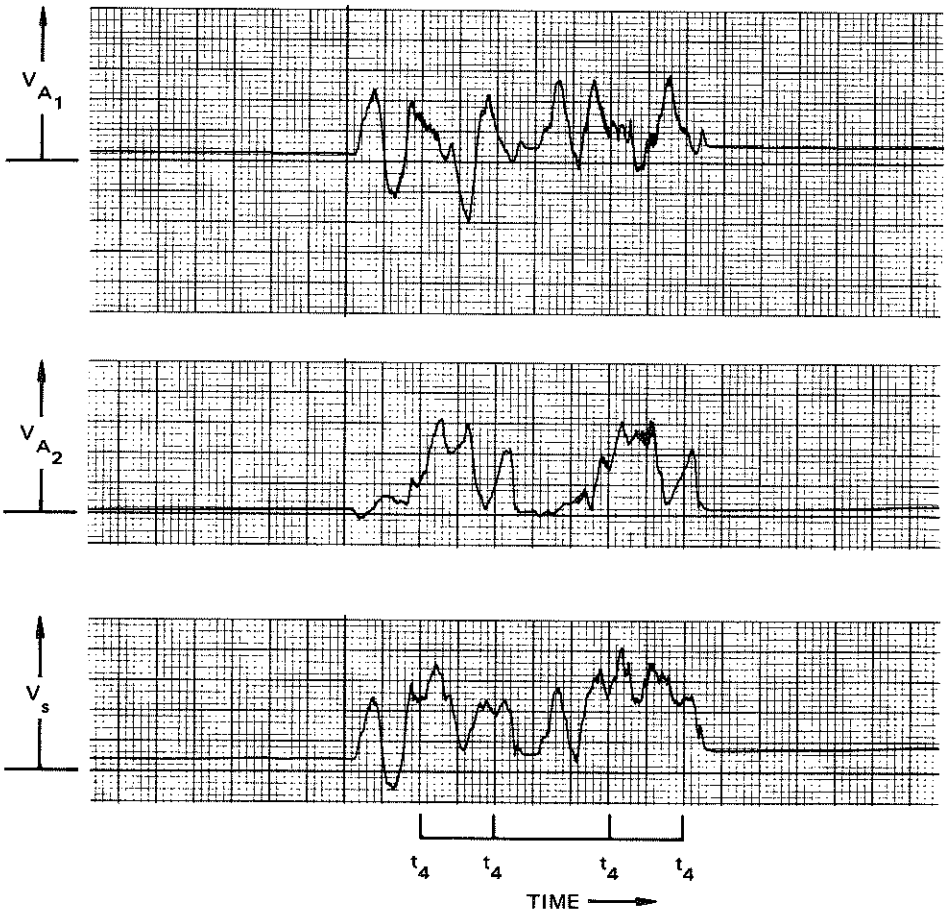

FIGURE XI-3 TYPICAL SIGNALS FROM STRAIN GAGES ON LEVER ARMS

been argued in Sections IV and VIII, "Design of Strain Gage Mounting" and "Calibration Results," respectively, that the sum of the two signals,

$$V_s = V_{A1} + V_{A2} \tag{3}$$

will be more directly related to retardation.

As discussed in Section B above, the time, t_4, corresponds to a wheel being opposite the second lever arm. Shown in Figure XI-3 are the retarder signals generated during the passage of four wheels through the retarder. The time, t_4, has been indicated for each wheel. Referring to the figure, the signal, V_s, is varying rapidly as a wheel is entering the retarder and as it is leaving the retarder. The signal is also varying rapidly as the wheel passes the center of the retarder, but is relatively constant when the wheel is near either one of the lever arms. The algorithm chosen for V_s is

$$I = (2 \text{ volt}^{-1})V_s(t_4) \tag{4}$$

Because V_s is relatively constant near t_4, the retardation index is relatively insensitive to small errors in finding t_4, which might occur in the data reduction.

The scattergram for the signal, V_s, is shown in Figure XI-4. Also shown in the figure is the line, ℓ, discussed in Appendix C. On the basis of this plot alone, it is clear that there is a strong correlation between the retardation index and measured retardation. The statistical analysis indicates that if the signal, V_s, were used for a slippery wheel detector, the probability of false alarms would be about 3.1 percent.

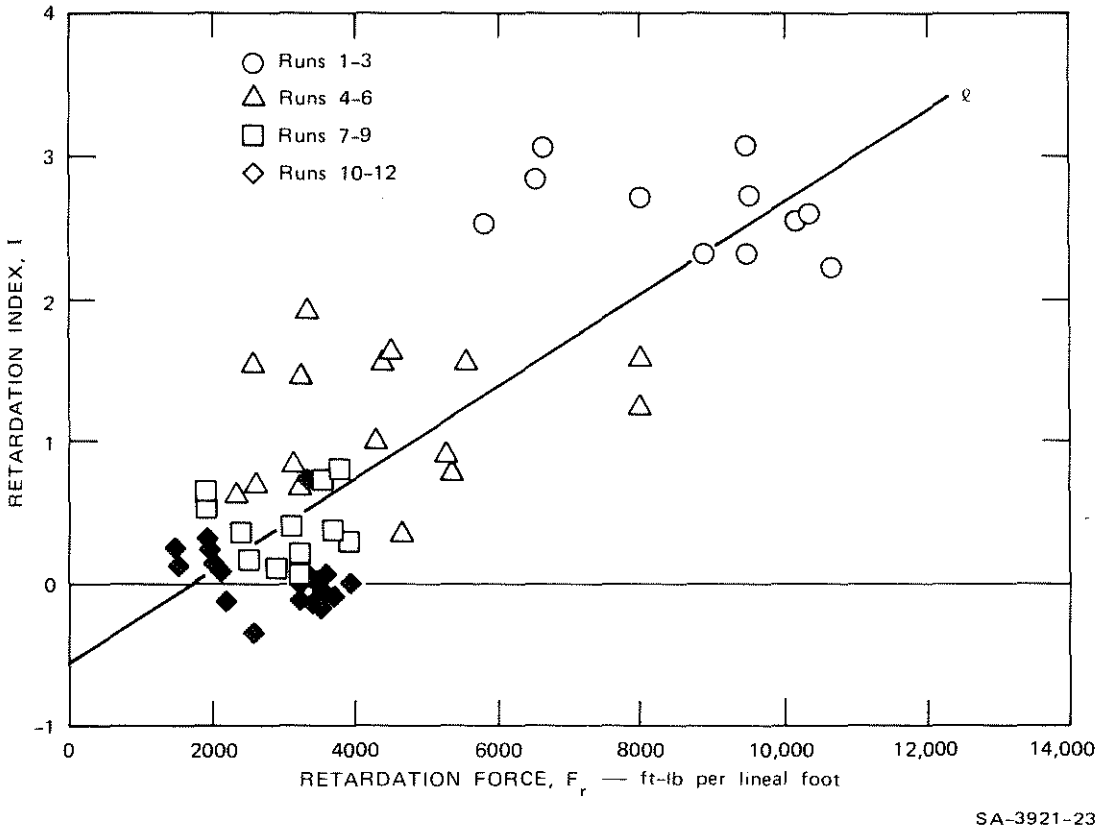

FIGURE XI-4 SCATTERGRAM FOR STRAIN GAGE SIGNAL, V_s

D. Accelerometer

A typical recorded signal from the accelerometer, V_A, is shown in Figure XI-5. The times, t_1, t_2, and t_3, described above in Section B, are also shown in the figure. Because of the limitations of the oscillographic recorder used to produce Figure XI-5, signal components above about 100 Hz are attenuated. Thus, Figure XI-5 represents the 0-to-100-Hz frequency band. The 100-to 1000-Hz and 100-to 10,000-Hz bands

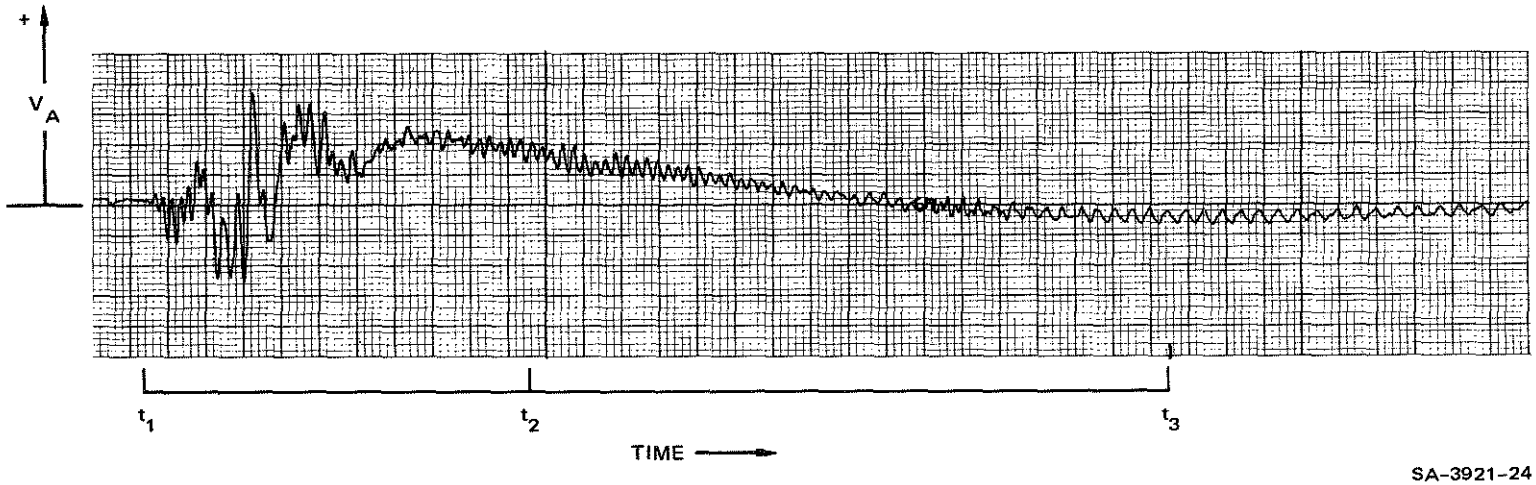

FIGURE XI-5 TYPICAL SIGNAL FROM ACCELEROMETER

were also investigated, but the 0-to 100-Hz band seemed to be most closely related to wheel slipperiness. Let V_A' be the signal components of V_A in the 10-to 100-Hz frequency band. The algorithm chosen for V_A is

$$I = \frac{(150 \text{ volt}^{-1})}{t_x} \int_{t_3 - \frac{t_x}{10}}^{t_3 + \frac{t_x}{10}} \left| V_A'(t) \right| dt \quad , \qquad (5)$$

where the time interval, t_x, is defined above in Section B. Stated in words, the retardation index is proportional to the average amplitude of V_A' while the wheel is near the center of the retarder.

The scattergram for the signal, V_A, is shown in Figure XI-6. Also shown in the figure is the line, ℓ, discussed in Appendix C. The statistical analysis indicates that if the signal, V_A, were used for a slippery wheel detector, the probability of false alarms would be about 8.4 percent.

E. Strain Gages on the Support Casting

A typical recorded signal from the strain gages on the support casting (V_B) is shown in Figure XI-7. As discussed in Section B above, the time, t_2, corresponds to a wheel being opposite the first lever arm. Shown in Figure XI-7 are the retarder signals generated during the passage of four wheels through the retarder. The time, t_2, has been indicated for each wheel. The algorithm chosen for V_B is

$$I = (4 \text{ volt}^{-1}) V_B(t_2) \quad . \qquad (6)$$

The scattergram for the signal, V_B, is shown in Figure XI-8. Also shown in the figure is the line, ℓ, discussed in Appendix C. The

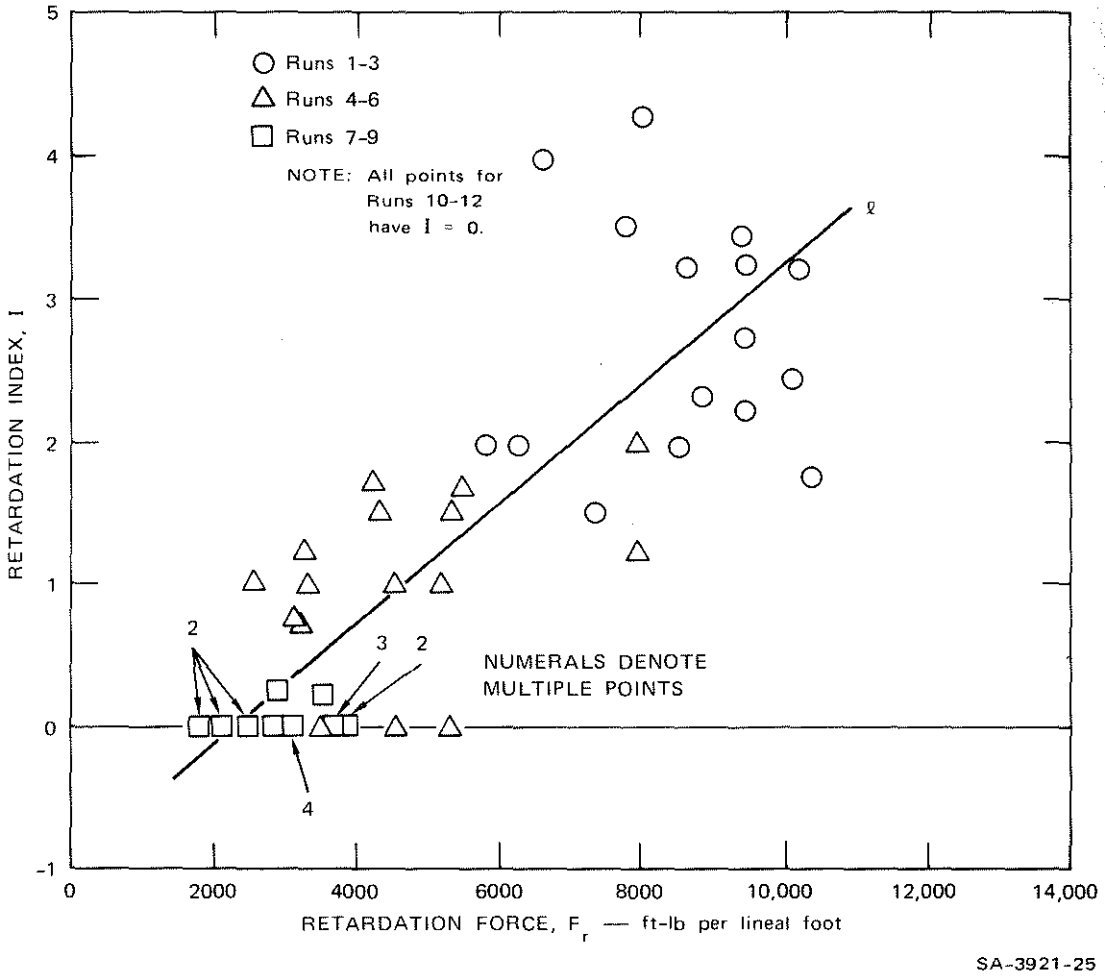

FIGURE XI-6 SCATTERGRAM FOR ACCELEROMETER SIGNAL

statistical analysis indicates that if the signal, V_B, were used for a slippery wheel detector, the probability of false alarms would be about 19 percent.

F. Statistical Analysis

A statistical analysis of the experimental data presented above is briefly described in this section. The mathematical details are contained

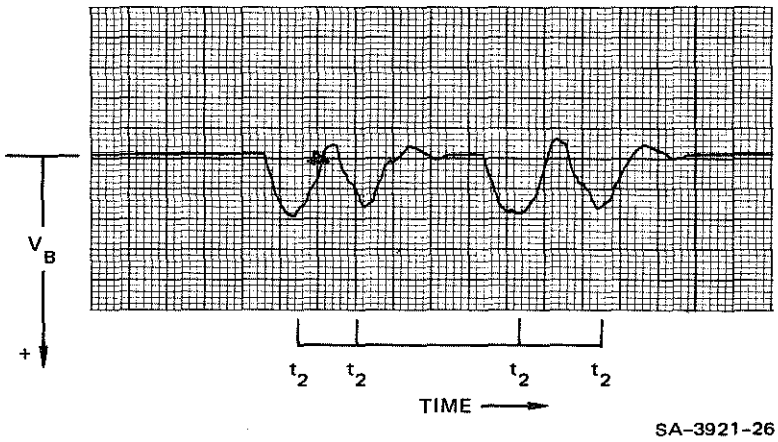

FIGURE XI-7 TYPICAL SIGNAL FROM STRAIN GAGES ON SUPPORT CASTING

in Appendix C. The statistical analysis is applied to each retarder signal in turn. The result in each case gives the percentage of "false alarms" (alarms given for cars that do not have slippery wheels) to be expected from a slippery wheel detector using that signal.

The statistical analysis considers the results of installation of slippery wheel detectors in the eight classification yards of the Southern Pacific system. It is assumed that an acceptable level of reliability of the detector would be equivalent to an average of one "missed alarm" in the eight Southern Pacific yards in 100 years. That is, on the average, the slippery wheel detectors would fail to warn of insufficient retardation only once in 100 years. This "missed alarm" level is not construed as an indication of the probability that another Houston-type accident would occur. The probability for such a repeat happening is substantially less than once in 100 years when traffic patterns and freight car mix probabilities are considered. In fact, to achieve a technically feasible operating detector, the "missed alarm" probability assumed in this analysis might be reduced appreciably while maintaining an extremely high probability for safe yard operation with respect to retardation.

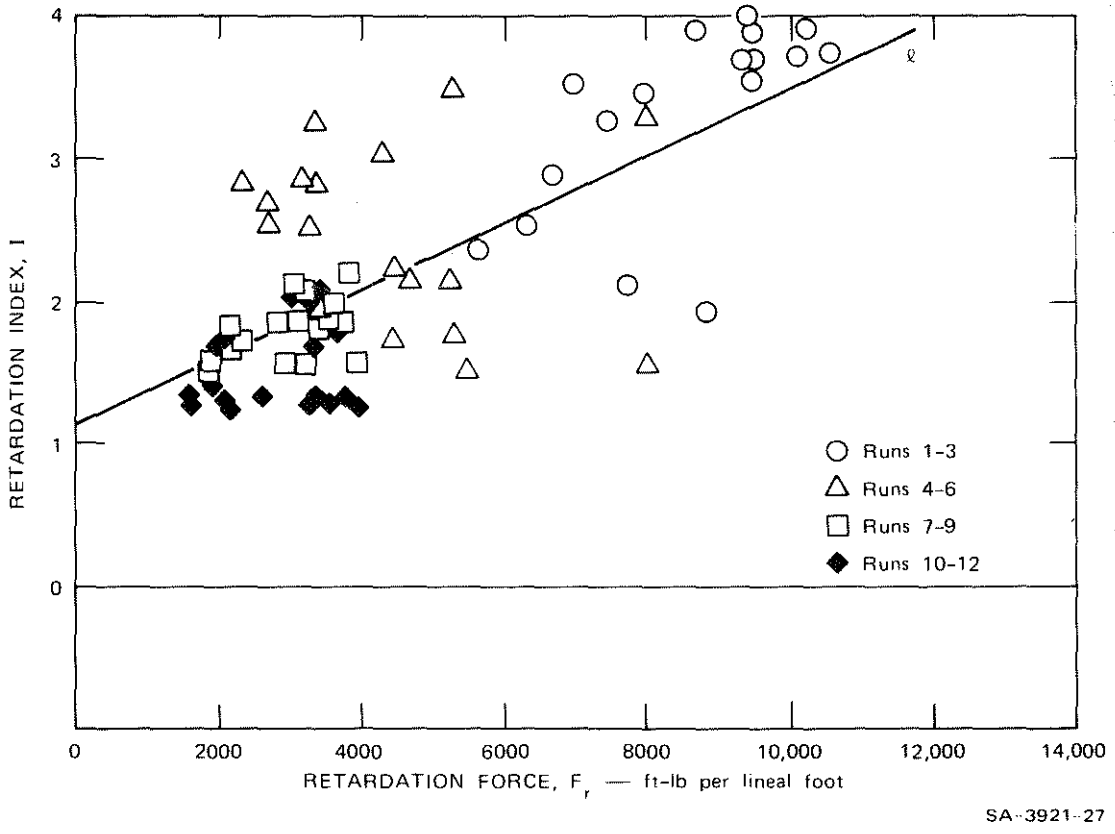

FIGURE XI-8 SCATTERGRAM FOR STRAIN GAGE SIGNAL, V_B

Therefore, the above criterion for reliability has been chosen arbitrarily for purposes of analysis and should not be construed as a recommendation.

The first step in the statistical analysis involves making a number of assumptions about the statistics of wheel "slipperiness" encountered in normal yard operations and about the statistics of the operation of the slippery wheel detector. Briefly, it is assumed that nonrepeatable

parameters, such as wheel "slipperiness" can be described by the Gaussian probability distributions that are most nearly consistent with the experimental data.

Let N be the number of cars with slippery wheels that would be humped in the Southern Pacific yards in one year. The value of N is computed from the assumed Gaussian distribution of wheel slipperiness.

Let I_c be the "critical value" of the retardation index, I. For cars with a retardation index less than I_c, an alarm would be given to the yard operator by the slippery wheel detector, and presumably the car would not be humped. Using the above value of N, the value of I_c is computed that satisfies the above criterion of one missed alarm in 100 years.

Finally, the above value of I_c is used to compute the percentage of "false alarms" to be expected from the slippery wheel detector.

The limitations of the statistical analysis are discussed in Appendix C. While the results of the statistical analysis cannot be considered accurate in the absolute sense, they do give a good indication of the relative effectiveness of the different signals for slippery wheel detection. Before slippery wheel detectors are put into widespread use, the predictions of the statistical analysis should be verified with more extensive testing. This could be accomplished by using a slippery wheel detector in an active classification yard for a trial period.

G. Discussion

Refer to Table XI-2, which lists for each form of instrumentation the percentage of "false alarms," P_f, expected from a slippery wheel detector in normal service in an active classification yard. A "false alarm" is an alarm given by the slippery wheel detector for a car that would experience normal retardation in the yard's retarders. The values of P_f listed in Table XI-2 have been calculated using the data from the

Table XI-2

PROBABILITY OF FALSE ALARMS
PREDICTED FOR INSTRUMENTATION SCHEMES TESTED

Instrumentation Scheme	Probability of False Alarms %
Load Cell	0.84
Strain gages on lever arms	3.1
Accelerometer	8.4
Strain gages on support casting	19.0

field tests. Several assumptions were necessary to make this calculation possible:

(1) The distribution of retardation forces encountered in an active classification yard is Gaussian.

(2) The retardation forces measured on runs 1, 2, and 3 in the field tests are representative of retardations encountered in an active classification yard.

(3) The operation of the slippery wheel detector can be described by the linear regression analysis presented in Appendix C.

(4) In all cases of minimum retardation, the retardation is 1250 ft-lb per lineal foot. (This is a conservative assumption, made to simplify the analysis.)

(5) An acceptable level of reliability for a slippery wheel detector is one "missed alarm" in 100 years for the eight large Southern Pacific classification yards (i.e., if slippery wheel detectors were installed in these yards, on the average, the slippery wheel detectors would fail to warn of unsafe retardation only once in 100 years.) This safety criterion has been chosen arbitrarily to allow the example calculation of relative detector effectiveness, and should not be construed as a recommendation.

These assumptions could not be verified easily, so the numbers in Table XI-2 should not be taken too seriously. However, the same assumptions were made for each of the instrumentation signals, so the relative values of false alarms shown in the figure can be considered meaningful.

For example, the percentage of false alarms in Table XI-2 for the load cell is 0.84 percent and for the accelerometer is 8.4 percent. If a load cell were used in a slippery wheel detector in an active classification yard, the percentage of false alarms could conceivably be greater or less than the 0.84 percent predicted. Whatever the percentage of false alarms from the detector using the load cell was, it would be safe to say that the percentage of false alarms from a slippery wheel detector using an accelerometer would be considerably greater.

Railroad yard operation is expensive and delays caused by false alarms would be costly. It is believed that the cost of false alarms will be the dominant life-cycle cost of a slippery wheel detector. Therefore, a slippery wheel detector employing a load cell, which would give the minimum percentage of false alarms, is the preferred design. The minimum configuration for such a slippery wheel detector would be similar to the instrumented retarder used in the field tests with the following changes:

(1) Eliminate unnecessary insturmentation--strain gages and accelerometer.

(2) Replace springs with a hydraulic cylinder or other constant-force device.

(3) Replace ball joints with a type that is more impervious to dirt and grit.

(4) Install switches or proximity detectors near each lever arm to signal the location of a wheel in the retarder.

(5) Shorten the retarder so that the length of the straight section is 3 feet. This is necessary to guarantee that two wheels are never in the retarder at once, even in the the case of 3-axle trucks that have a very short axle spacing.

(6) Provide some means to deal with the possibility that a wheel might stop while in the retarder. If a wheel stops in the retarder, the output of the slippery wheel detector may not be accurate. If the detector were located where a wheel would never stop, this problem would be avoided. Alternately, a sensor could be employed to detect wheel velocity.

(7) Provide necessary signal processing and interface with existing manual and/or automatic control systems in the yard. It will be necessary to use the instrumented retarder signals from all the wheels of a car to determine if an alarm should be given for that car. To do this, the signal processor must know which wheels belong to which car.

XII CONCLUSIONS

A. Comparison of Retarder Instrumentation

The primary purpose of this work was to determine which form of retarder instrumentation would be best for use in a slippery wheel detector.

Based on data obtained from field tests complemented by theoretical analysis, the following list presents the methods in the order most likely to be technically feasible:

(1) Load cell

(2) Strain gages on lever arms

(3) Accelerometer

(4) Strain gages on support casting.

B. Technical Feasibility

A secondary goal of this work was to investigate the technical feasibility of the slippery wheel detector concept. While results of the field tests are encouraging, at least two aspects of technical feasibility remain to be demonstrated:

(1) The appropriate selection of I_c, the critical retardation index, will have to be made from extensive field tests. This index may vary substantially depending on retarder yard configuration, equipment, and operating procedures.

(2) Mathematical analysis; using gross assumptions, predicts a probability of false alarms for the best configuration of slippery wheel detector tested of 0.84 percent. Thus, we would expect that for every 10,000 cars humped, the slippery wheel detector would give approximately 84 false alarms. This rate of false alarms must be reduced significantly for slippery wheel detectors to be feasible.

(3) The probability of missed alarms, which is a measure of the reliability of a slippery wheel detector, must give reasonable assurance that the slippery wheel detector will furnish a proper indication of a slippery wheel condition. First, a performance must be chosen. In this report, a performance level corresponding to one missed alarm in 100 years in all the eight large classification yards of the Southern Pacific railroad has been used as an example. The choice of this performance level was arbitrary and should not be construed as a recommendation. For technical feasibility of the slippery wheel detector, the chosen performance level must be demonstrated. Field tests of the slippery wheel detector involved only six cars and were completed in one day. In view of the variability expected under different yard circumstances, much more extensive and prolonged testing will be required to demonstrate technical feasibility for a particular application.

Approaches to the demonstration of technical feasibility as described above are discussed in Section XIII, "Suggestions for Future Work."

XIII SUGGESTIONS FOR FUTURE WORK

A. Decreasing the Probability of False Alarms

For the slippery wheel detector to be feasible, the probability of false alarms must be reduced considerably from the 0.84 percent predicted from the field tests.

The nonrepeatability of a car's retardation in a conventional retarder sets a lower limit on the probability of false alarms, even with a hypothetical "ideal" slippery wheel detector. The ideal detector is discussed in Appendix C and the probability of false alarms expected from such a detector is found to be 4.8×10^{-3} percent. (This corresponds to approximately one false alarm for every 20,000 cars humped.) No real detector is likely to achieve this low probability of false alarms, but one would expect that with improvements in the present design this value could be approached. A number of suggestions for reducing the probability of false alarms are discussed below:

(1) A number of slippery wheel detectors could be connected to one signal processor. This concept will be called an "averaging detector" because the signal processor would take the average of the outputs from instruments on the several detectors to determine a car's retardation. This concept is discussed in Appendix C for the case of an averaging detector using load cell instrumentation. The retarder used for the field tests had one load cell connected to one of the retarder shoes. For this minimum configuration, the predicted probability of false alarms is 0.84 percent, which corresponds to an average of 84 false alarms for every 10,000 cars humped. An averaging detector could be employed that would be similar to the detector used in the field tests but that would have one load cell connected to each shoe. For this case, less than 0.1 percent false alarms are expected. (Ten false alarms for each

10,000 cars.) Further improvement can be had by using two retarders, each with two load cells. For this case, about 0.01 percent false alarms are expected. (One false alarm for each 10,000 cars.)

(2) A lightly loaded car does not require as much retardation as a fully loaded car. If the signal processor for the slippery wheel detector were connected to a car weighing device, the processor could give a warning signal that would depend on the output of the slippery wheel detector instrumentation and on the car's weight. This would result in fewer false alarms.

(3) A slippery wheel detector employing a load cell mounted as in Concept II, described in Section V, could be used. This concept was not tested, but more accurate indications are expected from this design. In Concept II, friction at retarder pivots would not degrade the performance as it would in the load cell mounting concept that was tested. A disadvantage of this design is that it would probably be more expensive to develop and install. However, as noted above, installation is not likely to be the dominant life-cycle cost of the detector.

(4) The probability of false alarms will depend on the capacity of the conventional retarders used in each classification yard. For the purposes of this report, a safety factor of 2 was assumed for the yard's retarders. If the retarders exerted one-half the retardation claimed by the manufacturer, even the most heavily loaded car would not exit at an unsafe speed. The safety factor can be increased indefinitely by installing more retarders. As the safety factor is increased, the probability of false alarms will decrease.

(5) A probability of missed alarms which would correspond to an average of one missed alarm in 100 years in the eight large classification yards of the Southern Pacific Transportation Company was used as an example in this report. This probability of missed alarms is more conservative than it may at first seem. A missed alarm does not necessarily result in a disaster. Accidents, such as the recent explosion in Southern Pacific's Houston yard, would occur only when there is unsafe retardation combined with other factors such as a fully loaded car and dangerous cargo. Acceptance of a higher probability of missed alarms would result in fewer false alarms.

The above suggestions could be employed individually or in various combinations to reduce the probability of false alarms to an acceptable level.

B. System Design

Four major tasks remain before a slippery wheel detector is installed in an active classification yard for further testing. The first three tasks relate to the design of the entire slippery wheel detector system and are discussed in this section. The fourth task is the design of the test program itself which is discussed in Part C below.

First, a slippery wheel detector configuration must be chosen that is likely to give an acceptably small probability of false alarms. Some combination of the suggestions of Part A above should be chosen that, when used together, are likely to result in an acceptably low probability of false alarms.

After the detector configuration has been chosen, the signal processor for the detector must be designed. The signal processor would use the signals from retarder instruments, track switches, and possibly other sensors as inputs. The output of the signal processor would be a slippery wheel alarm and/or the value of the retardation index for each car.

The third task is the development of some method to verify that the slippery wheel detector and signal processor are not malfunctioning. The detector and signal processor should be tested periodically to ensure that "missed alarms" are not caused by unexpected equipment malfunction. A detector tester might consist of a device, similar to the calibration fixtures discussed in Section VII of this report, that applies a known load to the detector shoes. In addition, some self-testing capabilities might be built into the signal processor associated with the detector. For example, when a wheel is not in the detector, shunt calibration and zero drift tests could be performed automatically by the signal processor.

C. Demonstration of Safety

Two parameters effectively describe the performance of a slippery wheel detector. These are the probabilities of false alarms and of missed alarms. A practical slippery wheel detector would have a probability of false alarms that would correspond to about one false alarm per day in a large classification yard. This probability of false alarms could be easily demonstrated by use of a slippery wheel detector in a large yard for several days. For the slippery wheel detector to be proved technically feasible, its safety must also be demonstrated. This is equivalent to the problem of demonstrating a low probability of missed alarms while maintaining a practical probability of false alarms. This demonstration will be considerably more difficult than the simple demonstration of a practical probability of false alarms. Two approaches to this problem are discussed below.

A slippery wheel detector could be installed in an active classification yard. Any car that experienced an overspeed release from the yard's retarders would be noted. Likewise, cars for which the detector gave an alarm would also be noted. The probability of missed alarms, P_M can in theory be calculated from these data.

Unfortunately, this approach will require a very long testing period. For example, to demonstrate a probability of missed alarms corresponding to one missed alarm in the eight large Southern Pacific yards in 100 years, would require a testing program lasting at least 100 years. If testing were carried out in only one yard, 800 years would be required.

The second approach to the problem of demonstrating a low probability of missed alarms would be similar to the approach used in this report. A slippery wheel detector would be installed in an active classification yard. For each car, the retardation index from the detector would be recorded together with the retardation in the yard's retarders. A statistical analysis, possibly similar to the analysis presented in

in Appendix C, would be performed to predict the probability of missed alarms.

The testing program would be continued until sufficient data were accumulated so that there was an adequate level of confidence in the prediction of the statistical analysis. Mathematical methods exist to express the level of confidence as a percentage, if this is desired. Extending the length of the testing program will increase the level of confidence. It is expected that weather variations, especially precipitation, will affect retarder frictional properties. For this reason, the testing program should be continued for at least a year so that data are obtained during each season. The required duration of the testing program will be a matter of judgment, based on the level of confidence desired, and the time required to get a "representative" sample.

If this testing program is implemented, a considerable amount of data must be recorded and subsequently analyzed. The only practical way to accomplish this is with some form of automated data recording. Because many of the required sensors are already installed there, the Colton classification yard would be ideal for these tests. Shown in Figure XIII-1 is a block diagram of a data recording system that could be installed at the Colton yard. The minicomputer shown in the figure could, in principle, be the computer that is now installed at Colton. However, this would probably be impractical for a number of reasons:

(1) The computer would have to be reprogrammed, which would be very expensive.

(2) Additional input devices would have to be connected to the computer. This modification alone could be nearly as expensive as installing a second computer.

(3) At least during the installation and debugging of the data recording system, the automatic operation of the yard would be disrupted.

For these reasons, installation of a minicomputer dedicated to data recording for the slippery wheel detector is recommended. If properly

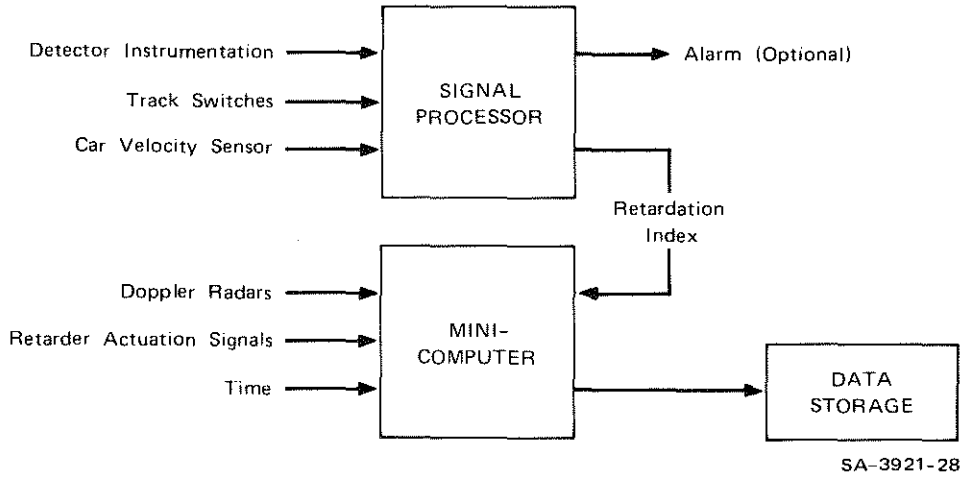

FIGURE XIII-1 DATA RECORDING SYSTEM, BLOCK DIAGRAM

implemented, this installation would not disrupt the yard operations. Failure of any part of the data recording system, including its computer, would not interfere with routine yard operation.

As discussed in Section XI, "Test Results and Discussion," the preferred design of retarder instrumentation may have to be abandoned if firction at the pivots becomes excessive. As a hedge against this possibility, it may be prudent to gather further data about a detector with strain gages on the lever arms. This could be most easily accomplished in conjunction with the demonstration of technical feasibility described above. A slippery wheel detector with strain gages on the lever arms would be installed near the load cell detector. Performance data would be recorded for both detectors. If the load cell detector proved unsuitable, consideration would turn to the strain gage detector. The data

necessary to evaluate the strain gage detector would be immediately available with no need for further testing. Similar reasoning indicates that concurrent testing of an "averaging detector," described above and in Appendix C, may be advisable.

Appendix A

ANALYSIS OF RETARDER LOADS

Appendix A

ANALYSIS OF RETARDER LOADS

The geometries of wheel rims and retarder shoes for the Abex retarder are shown in Figures A-1 and A-2. The area of contact between the wheel

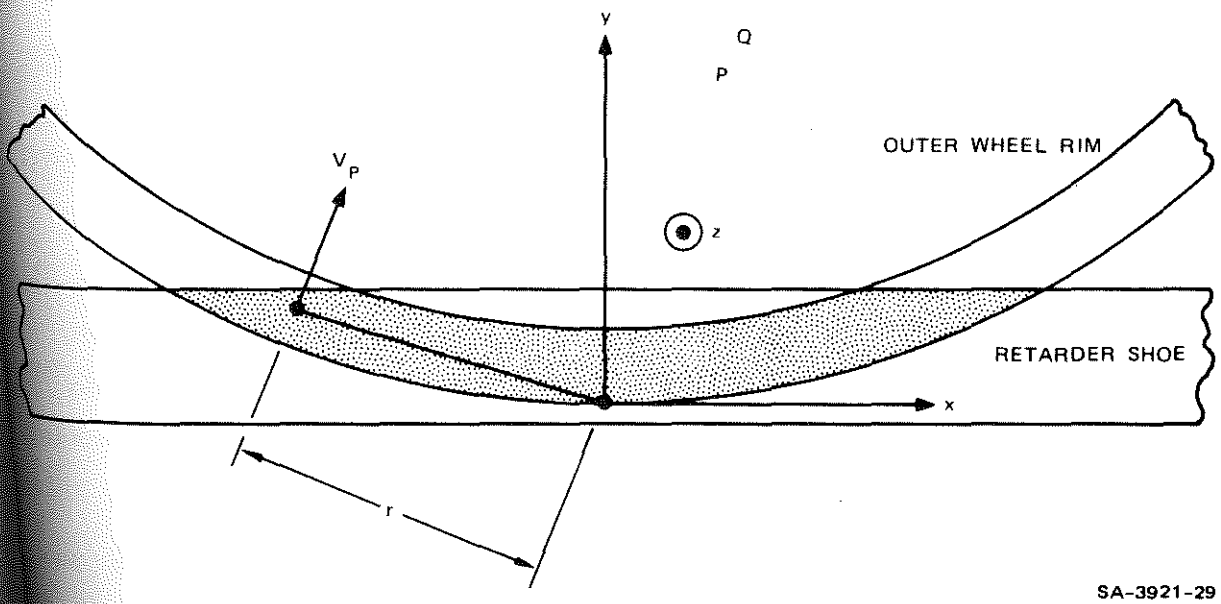

FIGURE A-1 OUTER RIM AND RETARDER SHOE GEOMETRY

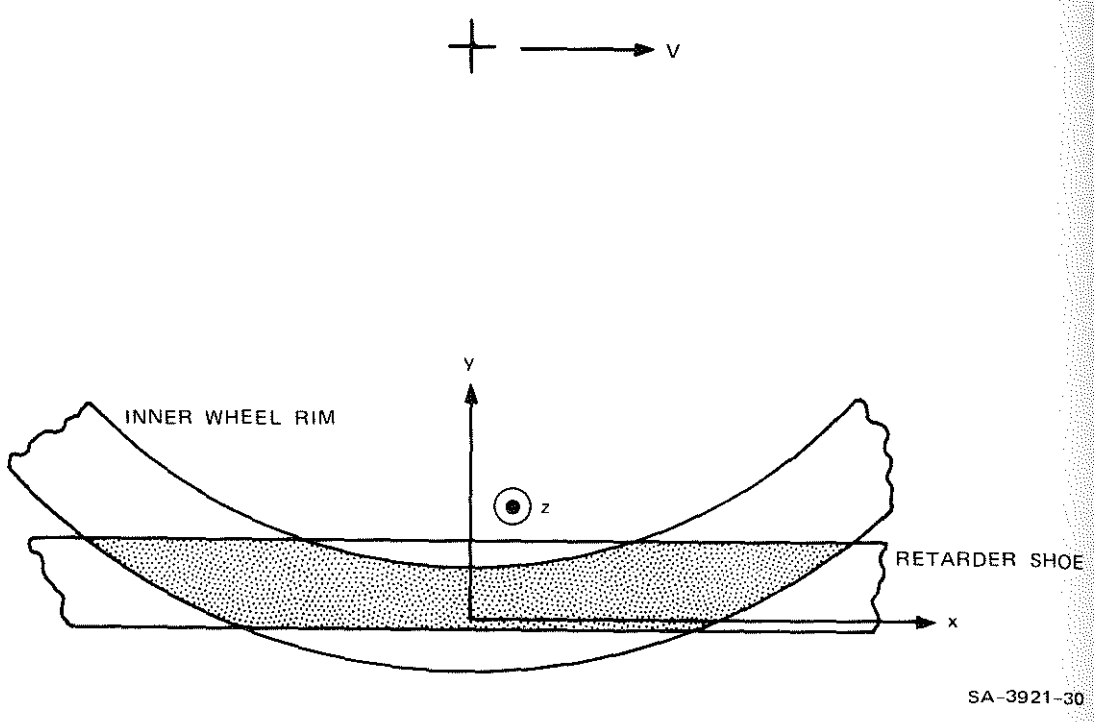

FIGURE A-2 INNER RIM AND RETARDER SHOE GEOMETRY

rim and the retarder shoe has been shaded. Note that inner and outer wheel rims have different geometries. In the figures, the origin of a Cartesian coordinate system has been chosen to coincide with the instantaneous point of contact between the wheel tread and the running rail, Q. The x axis has been chosen to coincide with the direction of motion of the car.

If there is no slippage between the wheel tread and the running rail, the point, Q, on the wheel tread, which contacts the rail, must have the same velocity as the rail, which is zero. The motion of any point, P, on the wheel can then be described as rotation about the point Q (see Figure A-1).

Assume that the interaction between the wheel rim and retarder shoe can be described by the Coulomb friction law. Then the force, $\vec{dF}$, exerted on a small element of retarder shoe face, dA, located at some point, P, is

$$\vec{dF} = \mu \frac{N}{A} \, dA \, \frac{\vec{V}_P}{|\vec{V}_P|} \quad , \tag{1}$$

where μ is the friction coefficient, N is the total normal force between the shoe and the rim, A is the total contact area, $\vec{V}_P$ is the velocity of the point P on the wheel. The notation $|\vec{V}|$ indicates the magnitude of vector, $\vec{V}$.

Let $\vec{F}$ be the total frictional force exerted on the shoe. Then

$$\vec{F} = \mu \frac{N}{A} \int_A \int \frac{\vec{V}_P}{|\vec{V}_P|} \, dA \quad . \tag{2}$$

Expressing $\vec{F}$ in terms of its components gives

$$\vec{F} = F_x \hat{i} + F_y \hat{j} = \hat{i} \, \mu \frac{N}{A} \int_A \int \frac{y}{\sqrt{x^2 + y^2}} \, dydx + \hat{j} \, \mu \frac{N}{A} \int_A \int \frac{x}{\sqrt{x^2 + y^2}} \, dydx \quad , \tag{3}$$

where $\hat{i}$, $\hat{j}$, and $\hat{k}$ are unit vectors in the x, y, and z directions, respectively. The area, A, is symmetrical about the y axis so the second term in Eq. (3) is zero, leaving

$$\vec{F} = \hat{i} \, \mu \frac{N}{A} \int_A \int \frac{y}{\sqrt{x^2 + y^2}} \, dydx = \hat{i} \mu N K_F \tag{4}$$

where K_F is a constant that depends only on retarder and wheel geometry. The integral in Eq. (4) has been evaluated numerically for a 38-inch, multiple-wear wheel in an Abex retarder giving

$$\vec{F} = \hat{i} \, \mu \, N(0.33) \tag{5}$$

for the outer rim, and

$$\vec{F} = \hat{i}\ \mu\ N(0.24) \tag{6}$$

for the inner rim.

Let $\vec{M}$ be the total twisting moment about Q exerted on the retarder shoe by the wheel (see Figure A-1). Then

$$\vec{M} = -\ \hat{k} \iint_A r\,|d\vec{F}| = -\ \hat{k}\ \mu\frac{N}{A}\iint_A \sqrt{x^2 + y^2}\ \ dxdy = -\hat{k}\mu N K_M \tag{7}$$

where K_M is a constant that depends only on retarder and wheel geometry. The integral in Eq. (7) has been evaluated numerically for a 38-inch, multiple-wear wheel in an Abex retarder giving

$$\vec{M} = -\ \hat{k}\ \mu\ N(3.8\ \text{inch}) \tag{8}$$

for the outer rim, and

$$\vec{M} = -\ \hat{k}\ \mu\ N(4.9\ \text{inch}) \tag{9}$$

for the inner rim.

The value of the normal force, N, depends on many variables. The Abex retarders are adjusted with a hydraulic jack placed between the retarder shoes at the location of each set of levers. The retarder is adjusted so that the jack is exerting approximately 22,000 pounds when the shoes are separated by one wheel width. As a single wheel passes through the retarder, the normal force will vary from a maximum of approximately 22,000 pounds when the wheel is at the location of a set of levers to a

minimum when the wheel is between two sets of levers. If there is more than one wheel in the retarder, the normal force on each wheel will be less than for one wheel alone. Wear of wheels and retarder shoes will further reduce the normal force.

The coefficient of friction, μ, also depends on many variables, the most important being the type of lubricant on the retarder shoes. Using a retarder manufacturer's published velocity head ratings, the retarder friction coefficient can be calculated. This calculation yields a value for μ of 0.1[6].

Assuming the maximum normal force ever encountered is 22,000 pounds and the maximum friction coefficient is 0.1, the maximum expected values of force and moment on the retarder shoe can be calculated from Eqs. (5), (6), (8), and (9):

$$\begin{aligned} F\ (\text{outer rim}) &= \quad 726\ \text{lb} \\ F\ (\text{inner rim}) &= \quad 528\ \text{lb} \\ M\ (\text{outer rim}) &= -\ 8{,}360\ \text{in-lb} \\ M\ (\text{inner rim}) &= -10{,}800\ \text{in-lb}. \end{aligned} \tag{10}$$

Shown in Figure A-3 is one retarder shoe with two levers attached. Also shown are a wheel and the forces and moments it exerts on the retarder shoe. These loads give rise to the reaction forces F_{1x}, F_{1y}, F_{2x}, and F_{2y} at the pivots. If there is sufficient radial clearance in the pivots, they will exert no z-axis moment on the levers, and this is assumed in the subsequent analysis. Other loads on the retarder shoe and levers, not shown in the figure, are z-axis forces at the pivots, at the attachment of the levers to the springs, and over the contact area between the wheel rim and the retarder shoe.

Since the retarder shoe is stationary in inertial space, its acceleration is zero, and hence the total of all forces and moments in each of the coordinate directions must be zero:

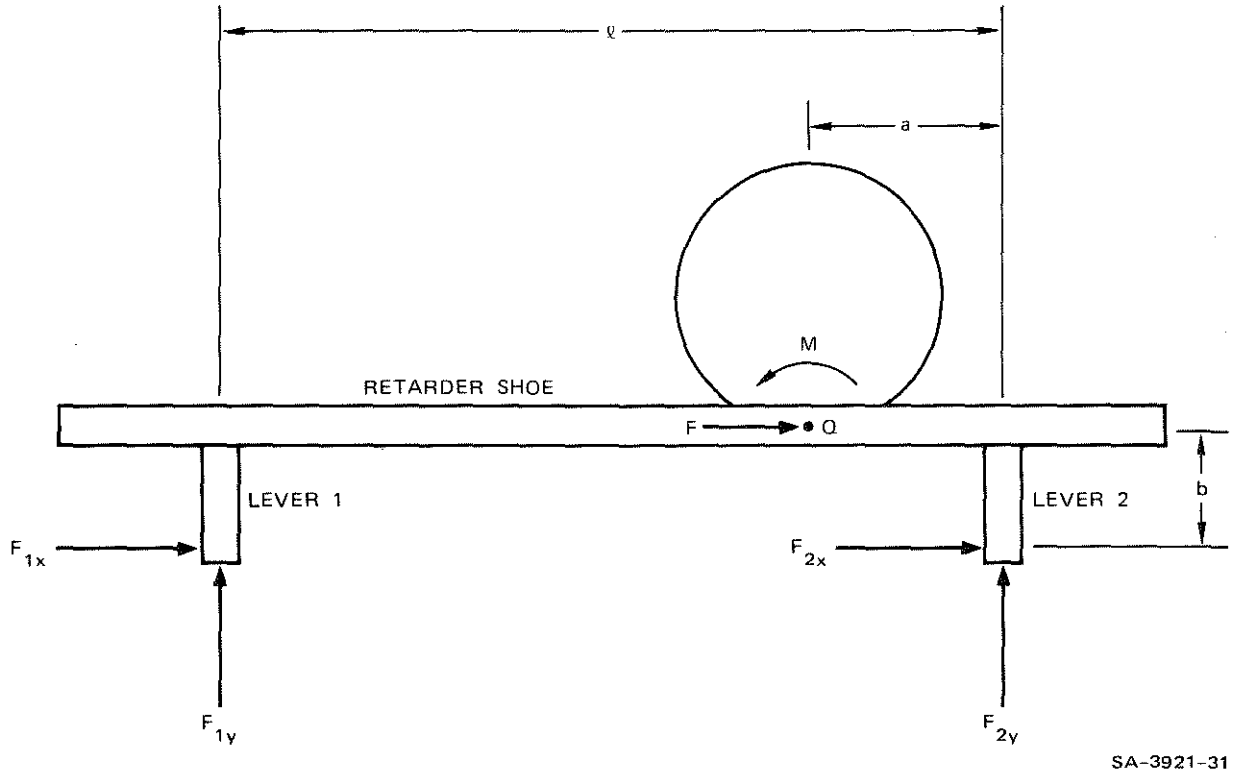

FIGURE A-3 RETARDER SHOE AND LEVERS

$$F_{1x} + F_{2x} + F = 0 \tag{11}$$

$$F_{1y} + F_{2y} = 0 \tag{12}$$

$$M - (\ell - a)\, F_{1y} + aF_{2y} + b(F_{1x} + F_{2x}) = 0 \quad . \tag{13}$$

If the pivot for one lever, for instance, lever 2, is designed with sufficient clearance in the x-direction and if this pivot also has negligible friction, then all longitudinal (x-direction) loads will be borne by lever 1:

$$F_{1x} \neq 0 \ , \ F_{2x} = 0 \tag{14}$$

Solving Eqs. (11), (12), (13), and (14) yields:

$$F_{1x} = -F \tag{15}$$

$$F_{2y} = -F_{1y} = \frac{bF-M}{\ell} \tag{16}$$

Referring to Eq. (10), 600 pounds and -9,000 in-lb are representative maximum values of F and M, respectively. For the Abex retarder:

$$b = 4.2 \text{ inch}$$
$$\ell = 50 \text{ inch.}$$

Using these values in Eqs. (15) and (16) gives

$$F_{1x} = -600 \text{ pounds}$$
$$F_{1y} = -230 \text{ pounds.} \tag{17}$$

A section of lever 1 is shown in Figure A-4. The lever has been broken near the end that attaches to the retarder shoe, and the bending moment transmitted by the lever, M_b, is shown. To satisfy static equilibrium (i.e., no acceleration of the lever), the net moment acting on the lever must be zero:

$$M_b - s_A F_{1x} = 0, \text{ or } M_b = s_A F_{1x} \quad . \tag{18}$$

Strain gages will be mounted at locations A and A′ shown in the figure. The stress, σ_y, at A′ is

$$\sigma_y \cong \frac{-M_b c_A}{I_A} \quad , \tag{19}$$

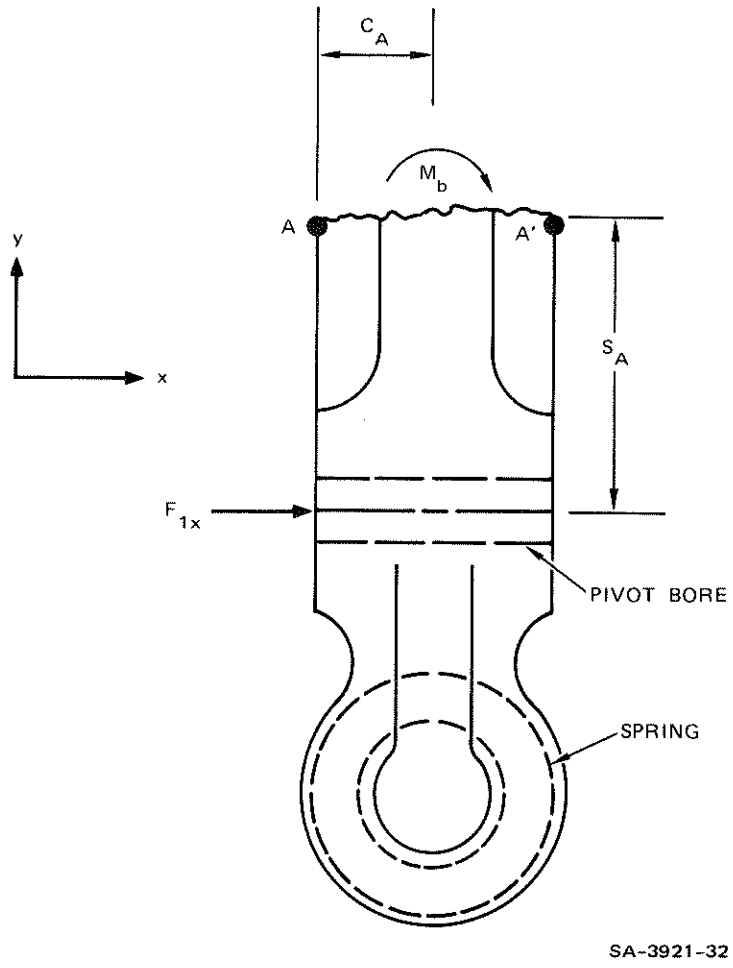

FIGURE A-4 LEVER 1

where I is the moment of inertia of the lever section between A and A'. The stress at A is the opposite of the stress at A'.

For the Abex lever:

$$I_A \cong 3.2 \text{ in}^4$$

$$s_A = 3.2 \text{ in}$$

$$c_A = 1.4 \text{ in} \quad .$$

Using Eqs. (17), (18), and (19) gives the maximum stress expected at A′,

$$\sigma_y \cong 840 \text{ psi} \tag{20}$$

Figure A-5 is a view of the support casting showing strain gage locations B and B′. Equal sharing of the load, F_{1y}, between the two sides of the casting has been assumed. Calculation of the stress at the gage locations is similar to the treatment above. The stress at B′ is

$$\sigma_z = \frac{-F_{1y} s_B c_B}{2I_B} \quad . \tag{21}$$

For the Abex support casting:

$$I_B \cong 15.6 \text{ in}^4$$

$$s_B = 2.5 \text{ in}$$

$$c_B = 2.5 \text{ in} \quad .$$

Using Eqs. (17) and (21) gives the maximum stress expected at B′,

$$\sigma_z \cong 46 \text{ psi} \quad . \tag{22}$$

Current foil strain gage technology is capable of resolving approximately 5 psi in cast iron. Semiconductor strain gages will resolve as little as 0.05 psi. The dynamic range, D, for a given gage type and location is

$$D = \frac{\sigma_{max}}{\sigma_r} \quad , \tag{23}$$

where σ_{max} is the maximum stress expected and σ_r is the resolvable stress.

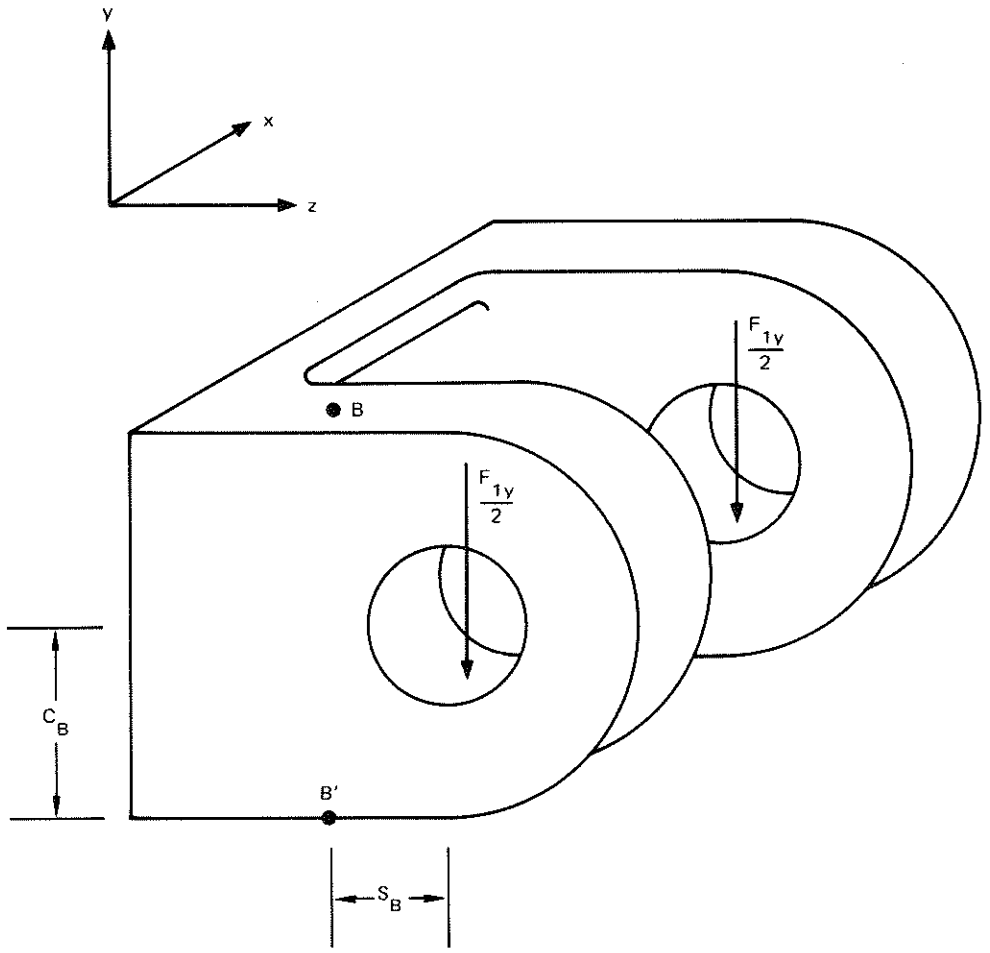

FIGURE A-5 SUPPORT CASTING

Values of D have been calculated using σ_{max} from Eqs. (20) and (21) and are tabulated in Table A-1.

Table A-1

DYNAMIC RANGE FOR VARIOUS GAGE TYPES AND LOCATIONS

Gage Locations	Gage Type	
	Foil	Semiconductor
On lever, A and A′	170	17,000
On support casting, B and B′	92	920

The strain gages are connected in bridge circuits as described in Section IX, Design of Instrumentation. In Appendix B, the equations for the output voltage, V_o, of a strain-gage bridge are derived. Let K be a constant and let $\sigma(P)$ denote the stress at some point, P. Then for small stresses and for gages at A and A′,

$$V_o = K\left[\sigma_y(A') - \sigma_y(A)\right] \quad , \tag{24}$$

and for gages at B and B′,

$$V_o = K\left[\sigma_z(B') - \sigma_z(B)\right] \quad . \tag{25}$$

The stress due to retardation loads $\vec{M}$ and $\vec{F}$ has the opposite sign at primed and unprimed locations:

$$\sigma_y(A) = -\sigma_y(A') \tag{26}$$

$$\sigma_z(B) = -\sigma_z(B') \quad . \tag{27}$$

Substitution of Eqs. (26) and (27) into Eqs. (24) and (25) gives

$$V_o = 2K\,\sigma_y(A') \tag{28}$$

$$V_o = 2K\,\sigma_z(B') \quad . \tag{29}$$

The only other significant cause of stress at A, A′, B, and B′ is the large normal force, N. A simple analysis shows that the stresses due to the normal force have the same sign at the strain gage locations:

$$\sigma_y(A) = \sigma_y(A') \tag{30}$$

$$\sigma_z(B) = \sigma_z(B') \quad . \tag{31}$$

Substitution of Eqs. (30) and (31) into Eqs. (24) and (25) gives

$$V_o = 0 \tag{32}$$

Thus, the outputs of the strain-gage bridges will be proportional to the loads, $\vec{F}$ and $\vec{M}$, correlated with retardation, and will be insensitive to the normal force, which is not correlated with retardation.

Appendix B

DESIGN CALCULATIONS FOR STRAIN GAGE BRIDGES

Appendix B

DESIGN CALCULATIONS FOR STRAIN GAGE BRIDGES

Shown in Figure IV-1 of the report is a schematic of a two-gage bridge circuit employing strain gages R1 and R2. The output voltage of the circuit, V_o, is given by the well-known voltage divider relationship

$$V_o = V_i\left[\frac{R_2}{R_1 + R_2}\right] \quad , \tag{1}$$

where V_i is the input voltage.

The resistance of a strain gage, R, is a function of its strain:

$$R = R_o[1 + \epsilon(G.F.)] \quad , \tag{2}$$

where ϵ is the strain, R_o is the nominal gage resistance, and G.F. is the "Gage Factor," a property of the gage.

Let ϵ_1 and ϵ_2 be the strains in gages R_1 and R_2, respectively. Combining Eqs. (1) and (2) yields

$$V_o = V_i\left[\frac{1 + \epsilon_2(G.F.)}{2 + (\epsilon_1 + \epsilon_2)\ (G.F.)}\right] \quad . \tag{3}$$

All strain gages mounted on the retarder will be placed so that the load of interest will produce equal and opposite strains in the two gages of each bridge (see Appendix A):

$$\epsilon_1 = -\epsilon_2 \quad . \tag{4}$$

Substitution of Eq. (4) in Eq. (3) yields

$$V_o = \frac{V_i}{2}[1 + \epsilon_2(G.F.)] \quad . \tag{5}$$

An advantage of the two-gage bridge is that it can be insensitive to temperature changes in the structure being gaged. The thermal conductivity of the retarder parts being gaged is so large that the temperatures at the two gages in each bridge will be very nearly equal. The change in strain, $\Delta\epsilon$, at any point in a structure due to a temperature change, ΔT, is given by

$$\Delta\epsilon = \alpha\Delta T \tag{6}$$

where α is the thermal expansion coefficient of the material. If the retarder's temperature changes by a (nonzero) amount ΔT, substitution of Eq. (6) in Eq. (3) gives

$$\Delta V = 0 \tag{7}$$

where ΔV is the change in bridge output voltage due to the temperature change ΔT.

Figure B-1 is the schematic of a four-gage bridge circuit. This configuration is easily analyzed by treating it as two two-gage bridges with a common input voltage. For example, there are four gages mounted on the support casting and connected in a four-gage bridge circuit. Let ϵ_2 and ϵ_3 be the strains in gages R_2 and R_3, respectively, then by Eq. (5),

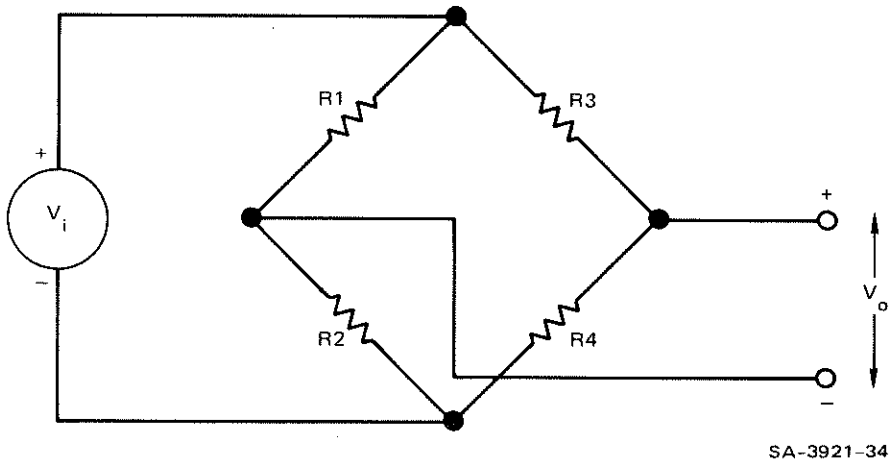

FIGURE B-1 FOUR-GAGE BRIDGE CIRCUIT

$$V_o = \frac{V_i}{2}(\epsilon_2 + \epsilon_3)\ (G.F.) \quad . \tag{8}$$

Stress, σ, and strain at any point in a structure are related by Young's modulus, E, which is a property of the structural material:

$$\epsilon = \frac{\sigma}{E} \quad . \tag{9}$$

Using Eqs. (8) and (9) together with the equations of Appendix A, the relation between the output voltage of the bridge on the support casting and the force, F_{1y}, can be derived:

$$V_0 = \left[\frac{V_i s_B c_B (G.F.)}{2\ I_B E}\right] F_{1y} \quad . \tag{10}$$

Appendix C

STATISTICAL ANALYSIS

Appendix C

STATISTICAL ANALYSIS

The following analysis employs the principles of probabilistic design that are described in recent publications.[7,8] To employ the probabilistic design equations, it is necessary to make certain assumptions about the physical system being modeled. In the following analysis, these assumptions will not be rigorously justified because this would be either impossible or at least expensive. While based on assumptions that can be questioned, the analysis is still useful because it allows us to deal with our uncertainty in a "rational" manner. Assumptions are explicitly stated and can be explicitly questioned. Furthermore, since essentially the same assumptions are made for the analysis of each signal, comparisons between signals can be made which are relatively independent of the assumptions in the model. This is highly desirable since one of the primary goals of this work is to compare the usefulness of the different signals for slippery wheel detection.

The limitations of the statistical analysis should be apparent. In particular, the results of this analysis should not be considered accurate in the absolute sense. Before slippery wheel detectors are put into widespread use, the predictions of the statistical analysis should be verified with more extensive testing. This could be accomplished by using a slippery wheel detector in an active classification yard for a trial period.

The follosing analysis makes frequent use of the Gaussian or "normal" probability distribution, which is described in most elementary statistics texts.[9,10] The distribution is described by two parameters,

the "mean" and "standard deviation," μ and σ. If x is a Gaussian random variable, and f(x) is the probability density function, then

$$f(x) = \frac{1}{\sigma\sqrt{2\pi}} e^{-\frac{1}{2}\left(\frac{x-\mu}{\sigma}\right)^2} \quad . \tag{1}$$

Probabilities are found by taking areas under the probability density function. For instance, the probability that x is greater than or equal to x_o is

$$Pr(x \geq x_o) = \int_{\infty}^{x_o} f(x)dx \quad . \tag{2}$$

The integral does not have a closed form, but the value of the integral can be found from many published tables.[11,12] To use these tables, the distribution is transformed to a "standardized distribution."[13] The limits of integration in the standardized distribution are given by the variable, u, defined

$$u \equiv \frac{x_o - \mu}{\sigma} \quad , \tag{3}$$

where x_o is the limit of integration.

Let x be a random variable and let x_i be the i^{th} observation of x. Then the two parameters, μ and σ, which describe the best Gaussian approximation to x are given by

$$\mu = \frac{1}{n}\sum_{i=1}^{n} x_i \tag{4}$$

and

$$\sigma = \left[\frac{1}{n-1}\sum_{i=1}^{n}(x_i - \mu)^2\right]^{1/2}$$

$$= \left(\frac{1}{n-1}\sum_{i=1}^{n} x_i^2 - \frac{n}{n-1}\mu^2\right)^{1/2} \qquad (5)$$

where n is the total number of observations.[14] The "coefficient of variation," C, is defined[15]

$$C \equiv \frac{\sigma}{\mu} \quad . \qquad (6)$$

This parameter can be considered a measure of nonrepeatability.

After the retardation indices for a given signal have been computed as described in Section XI of the report, "Test Results and Discussion," they are plotted against the retardation measured in the conventional retarder. Figure XI-1 is an example of such a plot. This plot, known as a "scattergram," quickly reveals the relationship between the retardation index and the measured retardation. A low amount of "scatter" (points nearly all on a single, straight line) is indicative of a signal which could be a "good" indicator of a slippery wheel. It should be apparent that even the "best" signals will show some scatter. This is because of the basic nonrepeatability of a car's retardation. Shown in Table XI-1 are the retardations measured by Southern Pacific in the conventional retarder. On runs 1, 2, and 3, the car wheels were not lubricated or tampered with in any way, but it is apparent from the table that the measured retardation is not very repeatable among these runs.

Consider the following experiment. A car is released at the crest and its retardation in the conventional retarder is measured. Assume the measured retardation is 8000 ft-lb per lineal foot. If the experiment were repeated, it is highly likely that the measured retardation would differ from the previously measured 8000 ft-lb per lineal foot. If we were to attempt to predict the measured retardation for a repeat of the experiment, the statistical variation from this measured value would need to be known.

Using Eqs. (4), (5), and (6), the parameters μ, σ, and C were computed for each car from the data of Table XI-1 for runs 1, 2, and 3. The results are presented in Table C-1. The average coefficient of variation is obtained by applying Eq. (4) to the coefficient of variation of Table C-1. The computed value is 7.05 percent. Therefore, we would expect

Table C-1

STATISTICAL DATA DEMONSTRATING VARIATIONS IN RUNS 1, 2, AND 3*

Car Number	μ ft-lb per lineal foot	σ ft-lb per lineal foot	C (%)
1	9527	613	6.4
2	7253	621	8.6
3	9800	350	3.6
4	9883	447	4.5
5	6523	803	12.3
6	8447	582	6.9
Average			7.05

*See text.

that even for the "best" signals, the scatter in a plot such as Figure XI-1 would be about 7 percent.

Figure C-1 is a histogram (bar graph) of the retardations measured on runs 1, 2, and 3 from Figure XI-1. Superimposed on the histogram is

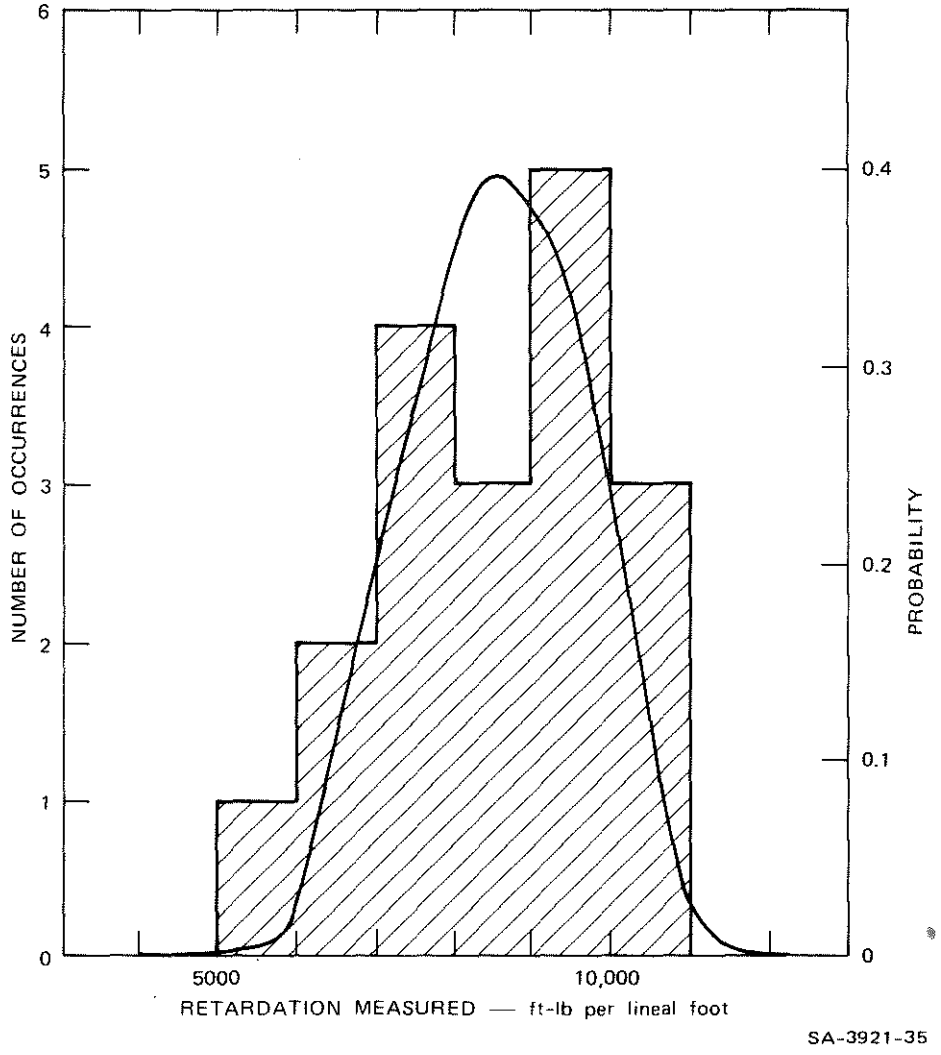

FIGURE C-1 HISTOGRAM OF MEASURED RETARDATION ON RUNS 1, 2, AND 3

the Gaussian probability distribution (smooth curve) which most closely approximates the histogram. Using the data from all cars on runs 1, 2, and 3 in Table XI-1, the parameters that describe the Gaussian

distribution of Figure C-1 were calculated using Eqs. (4) and (5). The results are

$$\mu_{F_r} = 8570 \text{ ft-lb per lineal foot}$$

and

$$\sigma_{F_r} = 1420 \text{ ft-lb per lineal foot} \qquad (7)$$

We will assume that the distribution of retardation forces in an active yard is given by this Gaussian distribution. Using the values of Eq. (7) in Eq. (6) gives a coefficient of variation of 17 percent. This coefficient differs from the value of 7.05 percent in Table C-1 because in Eq. (7), the distribution of retardations for all cars is considered. In Table C-1, the distribution of retardations for each car is considered separately.

The process of finding a single line, ℓ, which is the best fit of scattered data as shown in Figure XI-2, is known as linear regression analysis and is described in statistics texts.[16] Let x_i and y_i be the i^{th} observation of correlated random variables x and y. Let n be the total number of observations and define the following intermediate variables:

$$\mu_x \equiv \frac{1}{n} \sum_{i=1}^{n} x_i$$

$$\mu_y \equiv \frac{1}{n} \sum_{i=1}^{n} y_i$$

$$\sigma_x \equiv \left[\frac{1}{n-1} \sum_{i=1}^{n} (x_i - \mu_x)^2 \right]^{1/2}$$

$$\sigma_y \equiv \left[\frac{1}{n-1}\sum_{i=1}^{n}(y_i - \mu_y)^2\right]^{1/2}$$

$$\sigma_{xy} \equiv \frac{1}{n-1}\sum_{i=1}^{n}(x_i - \mu_x)(y_i - \mu_y) \qquad (8)$$

The parameters, b_0 and b_1 which describe the line, ℓ, are given by

$$b_1 = \frac{\sigma_{xy}}{\sigma_x^2} \qquad (9)$$

and

$$b_0 = \mu_y - b_1\mu_x \qquad (10)$$

The equation of the line, ℓ, is

$$y = b_0 + b_1 x \quad . \qquad (11)$$

The parameter, s, is a measure of the scatter of the data, and is given by

$$s = \left[\left(\frac{n-1}{n-2}\right)(\sigma_y^2 - b_1^2\sigma_x^2)\right]^{1/2} \qquad (12)$$

This parameter is analagous to the standard deviation, σ, for the single variable case.

We will assume that the retardation index (which corresponds to the variable, y, above) is a random variable given by

$$y_i = b_o + b_1 x_i + e_i \quad , \qquad (13)$$

where e_i is a random variable with

$$\mu_e = 0 \text{ and } \sigma_e = s \tag{14}$$

and x is the retardation force. The computed values of the parameters b_o, b_1, and s for the retarder signals recorded during the field tests are listed in Table C-2.

Equations (13) and (14) are illustrated in Figure C-2. For those cars with retardation in the conventional retarder equal to F_1, the distribution of retardation indices is given by the curve $P(F_1)$ in the figure. Similarly, the distribution for any other value of retardation such as F_2 is given by a similar distribution, $P(F_2)$ also shown in the figure.

The conventional retarder used in these tests is claimed by the manufacturer to exert a minimum retardation force of 2500 ft-lb per lineal foot. Classification yards are commonly designed with a safety factor of 2. That is, if the conventional retarder exerts a retardation force of at least 1250 ft-lb per lineal foot, then exit speeds of cars from this retarder are within the design parameters of the retarder. We will define the "minimum retardation" as 1250 ft-lb per lineal foot.

The large classification yards of the Southern Pacific Railroad together with their average traffic are listed below:

Yard	Traffic
Los Angeles (Taylor)	1,800 cars/day
Eugene	2,300 cars/day
Roseville	3,000 cars/day
Colton	3,000 cars/day
Houston	3,100 cars/day
Pine Bluff	2,200 cars/day
City of Industry	1,000 cars/day
Beaumont	800 cars/day
Total	17,200 cars/day

Table C-2

STATISTICAL PARAMETERS

Parameter	Load Cell	Strain Gages on Lever Arms	Accelerometer	Strain Gages on Support Casting	Ideal Detector
b_o	-0.370	-0.557	-0.966	1.16	0.00
b_1 (lb^{-1})	3.36×10^{-4}	3.23×10^{-4}	4.14×10^{-4}	2.36×10^{-4}	3.00×10^{-4}
s	0.435	0.511	0.789	0.546	0.180
I_c	0.970	0.929	1.22	2.61	0.757
μ_I	2.5	2.2	2.6	3.2	2.6
σ_I	0.64	0.69	0.99	0.64	0.46
P_f	0.84%	3.1%	8.4%	19%	0.0048%

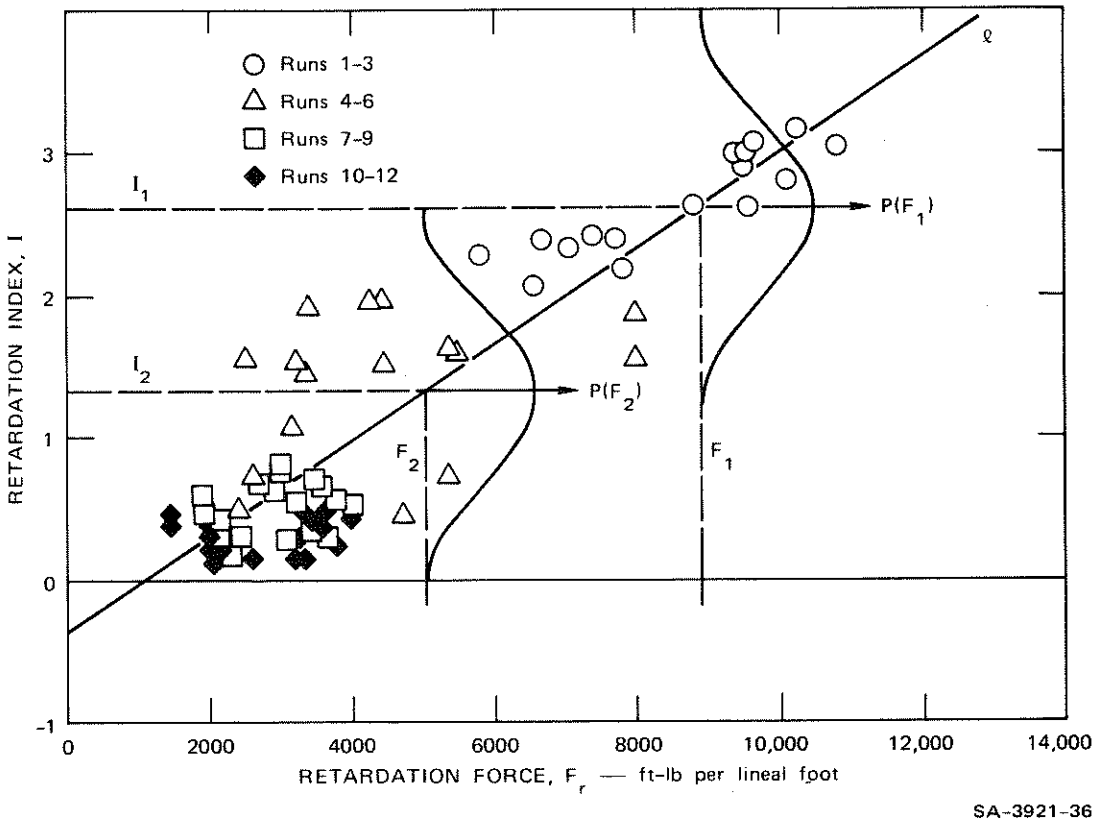

FIGURE C-2 SCATTERGRAM FOR LOAD CELL

Let N_T be the total number of cars humped in these yards in one year. The value of N_T is estimated

$$N_T \cong 17{,}200 \text{ cars/day} \times 350 \text{ days/year} \cong 6.0 \times 10^6 \text{ cars/year} . \quad (15)$$

"Minimum retardation" is defined as retardation less than or equal to 1250 ft-lb per lineal foot. Let N be the number of occurrences of minimum retardation in the large Southern Pacific yards in one year. The

parameter, N, is found from the Gaussian distribution of Figure C-2, and is given by

$$N = N_T \Pr(F_R \leq 1250 \text{ ft-lb per lineal foot}) \quad . \tag{16}$$

Converting to the standardized distribution, the parameter, u is found using Eq. (3):

$$u = \frac{x_o - \mu_{F_r}}{\sigma_{F_r}} = \frac{1250 \text{ lb} - 8520 \text{ lb}}{1420 \text{ lb}} = -5.12 \quad .$$

From the tables,[11]

$$\Pr(F_r \leq 1250) \cong 10^{-7} \tag{17}$$

Then using Eqs. (15), (16), and (17)

$$N = N_T \Pr(F_r \leq 1250) \cong 6.0 \times 10^6 \times 10^{-7} = 0.6 \quad . \tag{18}$$

To simplify the following analysis, we will assume that in all cases of minimum retardation, the retardation force is 1250 ft-lb per lineal foot. In fact, some cars may experience retardations of less than 1250 ft-lb per foot, but our assumption will yield conservative results and is therefore justified.

For the purposes of this analysis, we will consider the results of installation of slippery wheel detectors in the large Southern Pacific classification yards. We will assume that an aceeptable level of reliability would be equivalent to an average of one "missed alarm" in 100 years. That is, on the average, the slippery wheel detectors would fail to warn of slippery wheels only once in 100 years. This criterion has been chosen arbitrarily and should not be construed as a recommendation.

A critical value of retardation index, I_c, must be chosen. For cars with a retardation index less than I_c, an alarm would be given to the yard operator by the slippery wheel detector. Given the above assumptions, I_c can be calculated. It has been assumed that all cars which experience minimum retardation experience a retardation force of 1250 ft-lb per lineal foot. From Eq. (13), the distribution of retardation indices for these cars is a Gaussian distribution with

$$\mu_I = b_0 + b_1(1250 \text{ ft-lb per lineal foot}) \tag{19}$$

and

$$\sigma_I = s \quad . \tag{20}$$

This distribution is shown in Figure C-3 for the load cell signal.

Also shown in Figure C-3 is a chosen value of I_c. The area under the curve to the right of I_c is shown shaded and represents the probability, P_M, that an alarm will not be given for a car with slippery wheels (a "missed alarm"). For one missed alarm in 100 years,

$$P_M = \frac{1}{(100)N} \quad . \tag{21}$$

Using Eqs. (18) and (21) gives

$$P_M = 1.7 \times 10^{-2} = 1.7\% \quad . \tag{22}$$

The critical value of the retardation index, I_c, is chosen so that for the above distribution,

$$\Pr(I \geq I_c) = P_M \quad . \tag{23}$$

For the value of P_M given in Eq. (22), the value of u found in the tables[12] is

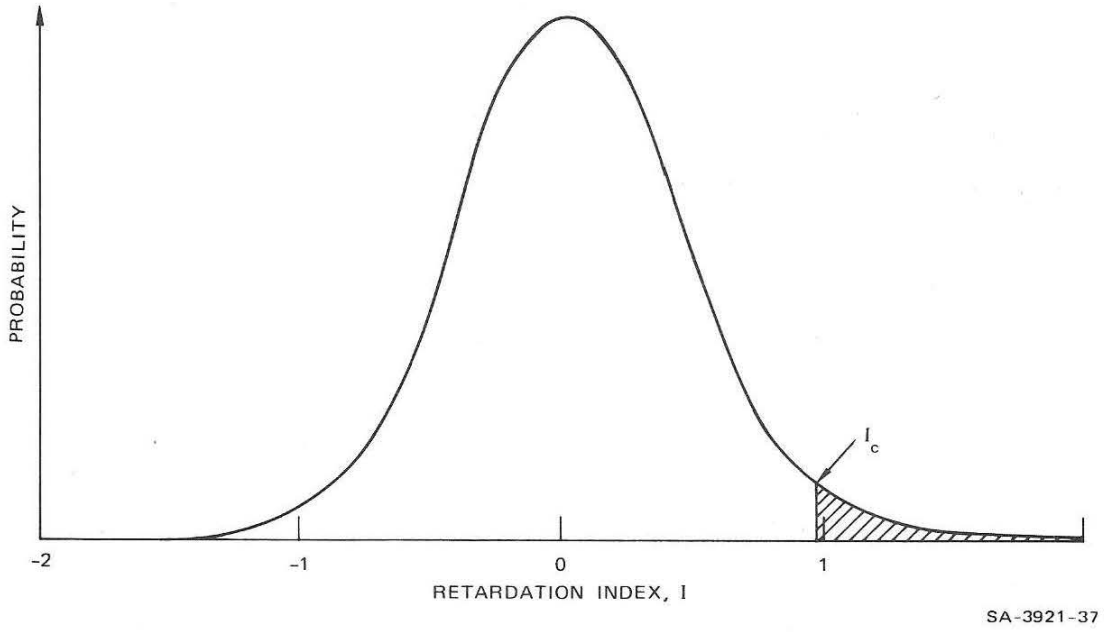

FIGURE C-3 PROBABILITY DISTRIBUTION OF RETARDATION INDEX FOR LOAD CELL SIGNAL FOR CARS WITH F_r = 1250 ft-lb PER LINEAL FOOT

$$u = 2.12 \quad . \tag{24}$$

Rewriting Eq. (3) with Eqs. (19), (20), and (24) gives

$$I_c = b_0 + b_1(1250 \text{ ft-lb per lineal foot}) + (2.12)s \quad . \tag{25}$$

The computed values of the parameter, I_c, for the retarder signals recorded during the field tests are listed in Table C-2.

Denote the Gaussian random variable, F_r, of Figure C-1 by its mean and standard deviation with the notation

$$F_r = (\mu_{F_r}, \sigma_{F_r}) \quad . \tag{26}$$

Similarly, the Gaussian random variable, e, is written

$$e = (\mu_e, \sigma_e) \quad . \tag{27}$$

Using the "algebra of random variables"[17] and Eqs. (26) and (27), Eq. (13) can be rewritten as follows:

$$I = b_0 + b_1 F_r + e = b_0 + b_1(\mu_{F_r}, \sigma_{F_r}) + (\mu_e, \sigma_e)$$

$$= b_0 + (b_1\mu_{F_r}, b_1\sigma_{F_r}) + (\mu_e, \sigma_e)$$

$$I = \left[b_0 + b_1\mu_{F_r} + \mu_e, (b_1^2\sigma_{F_r}^2 + \sigma_e^2)^{1/2}\right] \quad . \tag{28}$$

Thus, I is a Gaussian random variable with mean and standard deviation given by Eq. (28). Substituting from Eqs. (7) and (14) gives

$$I = (\mu_I, \sigma_I)$$

where

$$\mu_I = b_0 + b_1(8570 \text{ ft-lb per lineal foot})$$

$$\sigma_I = \left[b_1^2(2.02 \times 10^6 \text{ lb}^2) + s^2\right]^{1/2} \quad . \tag{29}$$

This curve is shown in Figure C-4 for the load cell signal. Unlike Figure C-3, which showed retardation indices for cars with minimum retardation only, Figure C-4 shows retardation indices for all cars. The computed

values of the parameters μ_I and σ_I from Eq. (29) for the retarder signals recorded during the field tests are listed in Table C-2.

An alarm is given for all cars for which the retardation index, I, is less than or equal to I_c. To find the probability of alarms, P_A, which is the area to the left of I_c shown shaded in Figure C-4, we must first

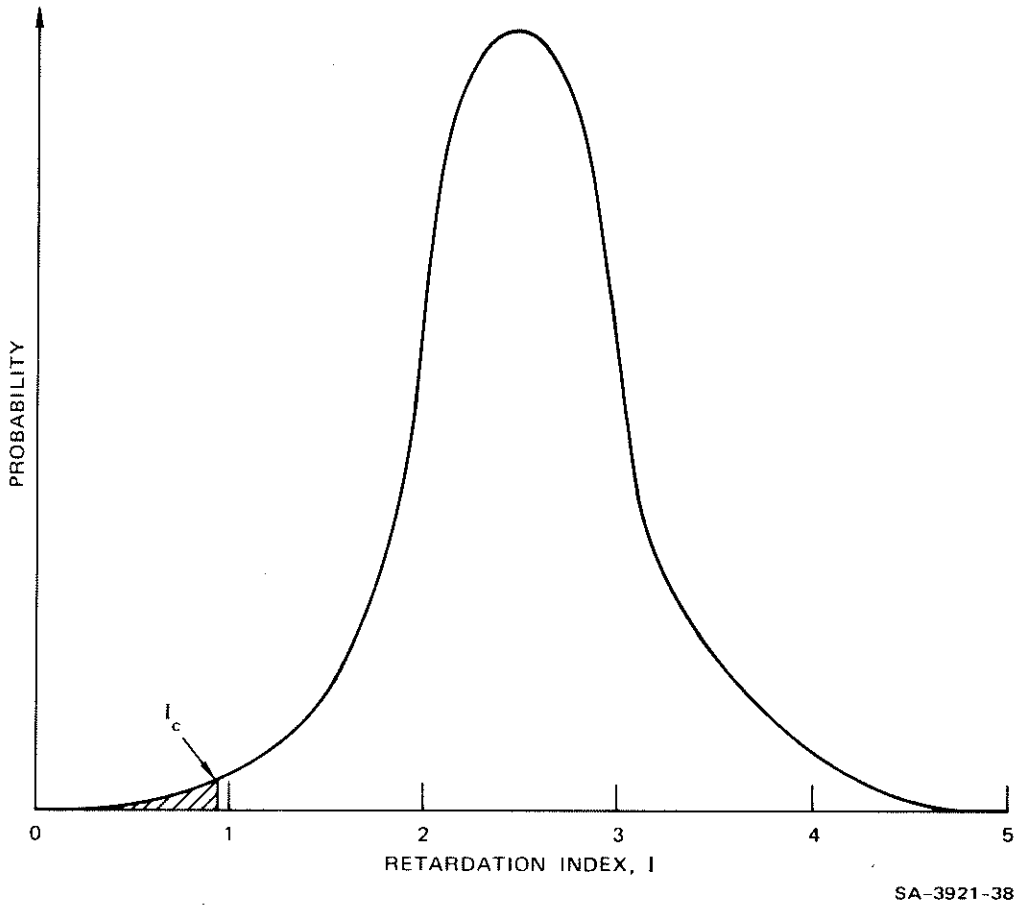

FIGURE C-4 PROBABILITY DISTRIBUTION OF RETARDATION INDEX FROM LOAD CELL SIGNAL FOR ALL CARS

convert to the standardized distribution. The parameter u, is given by Eq. (3),

$$u = \frac{I_c - \mu_I}{\sigma_I} \tag{30}$$

For the load cell signal,

$$u = \frac{0.970 - 2.5}{0.64} = -2.39 \quad .$$

From the tables,[12]

$$P_A = Pr(I \leq I_c) = 0.0084$$

for the load cell.

Let P_C be the probability of "correct alarms," alarms given for cars with slippery wheels and let P_F be the probability of "false alarms," alarms given for cars with normal wheel conditions;

$$P_A = P_C + P_F$$

or

$$P_F = P_A - P_C \tag{31}$$

The parameter, I_c, has been chosen to give an average of 1/100 missed alarm per year. The average number of correct alarms per year, N_c, is given by

$$N_c = N - (1/100) = 0.60 - 0.01 = 0.59 \quad , \tag{32}$$

and the probability of a correct alarm is

$$P_c = \frac{N_c}{N_T} \quad . \tag{33}$$

Substituting from Eqs. (15) and (32) gives

$$P_c = \frac{0.59}{6.0 \times 10^6} \cong 10^{-7} \quad . \tag{34}$$

For the load cell signal, using Eqs. (31) and (34) gives

$$P_F = 0.0084 - 10^{-7} = 0.0084 = 0.84\% \quad .$$

The computed values of the parameter P_F for each of the retarder signals recorded during the field tests are listed in Table C-2.

Consider a hypothetical "ideal" slippery wheel detector. This detector would consist of a retarder identical to the conventional retarders used in a classification yard. The retarder would be instrumented with "perfect" instruments that would measure the retardation exactly. Referring to Table C-1 and the accompanying discussion, the scattergram for an ideal slippery wheel detector would have a scatter, s, of about 7 percent. For example, assume that for the ideal detector,

$$b_0 = 0$$

and

$$b_1 = 3 \times 10^{-4} \text{ lb}^{-1} \quad . \tag{35}$$

For 7 percent scatter in retardation force, F_r,

$$(0.07)\mu_{F_r} = \frac{s}{b_1}$$

or (36)

$$s = (0.07)\mu_{F_r} b_1 = 0.07 \times 8570 \text{ lb} \times 3 \times 10^{-4} \text{ lb}^{-1} = 0.180 \quad .$$

Using the values of Eqs. (35) and (36), the values of the parameters I_c, μ_I, σ_I, and P_f for an "ideal" slippery wheel detector have been

calculated and are listed in Table C-2. The value of P_f for the ideal detector is 4.8×10^{-3} percent.

Consider a slippery wheel detector composed of a number of load cell-instrumented detectors, such as the one used in the field tests. Signal processing circuitry takes the average of the retardation indices reported by each detector, and this average becomes the retardation index for the car. This concept will be called an "averaging detector." For such a detector, the scatter, s, is given by[18,19]

$$S_A = \frac{1}{\sqrt{n}} S_L \tag{37}$$

where S_A denotes the scatter for the averaging detector, S_L is the scatter for the single detector using a load cell, and n is the number of single detectors used in the averaging detector. The values of the parameters b_0 and b_1 for the averaging detector will be identical with those of the single detectors.[18,19] Equation (37) was used to compute S_A for various values of n. The probability of false alarms, P_f, was then calculated for each case. The results are shown in Figure C-5 (solid line). Also shown in the figure is the value of P_f calculated above for an "ideal" slippery wheel detector. As discussed above, no slippery wheel detector could give a lower value of P_f than an ideal detector. As n is increased beyond 3, Eq. (37) is not applicable because the nonrepeatability of retardation begins to dominate the nonrepeatability of the retarder instrumentation. This effect is shown by the broken line in the figure.

This result has important implications for the technical feasibility of the slippery wheel detector. To be technically feasible, a detector employing a single load cell would probably give an excessive number of false alarms. Referring to Figure C-5, the probability of false alarms would be 0.84 percent for a detector employing a single load cell. If two load cells were used in an averaging detector, the probability of

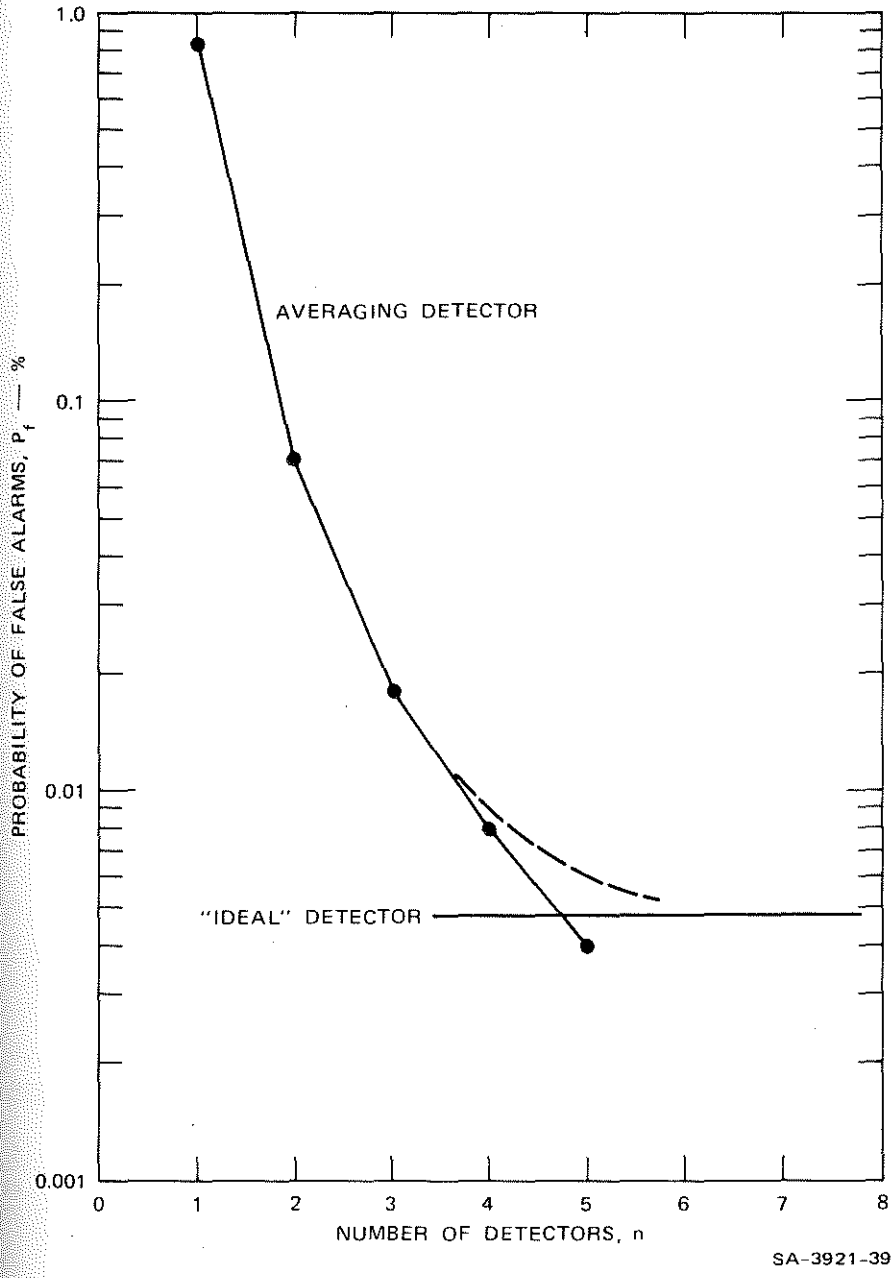

FIGURE C-5 PROBABILITY OF FALSE ALARM, P_f, FOR AVERAGING DETECTOR

false alarms would be reduced to about 0.07 percent. Using four load cells would further reduce the probability of false alarms to less than 0.01 percent. The indication is that an averaging detector using two to four load cells would not give an excessive number of false alarms and would be technically feasible.

REFERENCES

1. "Railroad Accident Report Hazardous Materials Accident at the Southern Pacific Transportation Company's Englewood Yard Houston, Texas, September 21, 1974," National Transportation Safety Board Report Number NTSB-RAR-75-7, adopted May 21, 1975.

2. Mechanical Behavior of Materials, F. A. McClintock and A. S. Argon, eds., p. 82 (Addison-Wesley, Reading, Massachusetts, 1966).

3. F. A. McClintock and A. S. Argon, op. cit. p. 397.

4. Robert L. Kiang, "Retarder Noise Study," SRI Final Report, p. 26 (29 January 1973).

5. Ralph Morrison, Grounding and Shielding in Instrumentation (John Wiley, 1967).

6. John T. Golden and Paul E. Stallings, "Conclusions and Recommendations of the Shell Oil Company," Before the Department of Transportation National Transportation Safety Board, p. 28, Docket No. SS-R-34 (January 6, 1975).

7. E. B. Haugen, Probabilistic Approaches to Design (John Wiley, 1968).

8. E. B. Haugen and P. H. Wirshing, "Probabilistic Design, Parts I-V," Machine Design, Vol. 27, Nos. 9, 11, 12, 13, and 14 (Penton Publishing, Cleveland, Ohio, 1975).

9. A. A. Afifi and S. P. Azen, Statistical Analysis A Computer Oriented Approach, pp. 305-307 (Academic Press, New York, 1972).

10. E. B. Haugen and P. H. Wirshing, "Probabilistic Design, Part II," Machine Design, Vol. 47, No. 11, p. 81 (Penton Publishing, Cleveland, Ohio, 1975).

11. E. B. Haugen and P. H. Wirshing, op. cit. p. 84.

12. Handbook of Chemistry and Physics, R. C. Weast, ed., p. A-106 to A-108 (The Chemical Rubber Company, Cleveland, Ohio, 1964).

13. E. B. Haugen and P. H. Wirshing, loc. cit.

14. E. B. Haugen and P. H. Wirshing, "Probabilistic Design, Part I," Machine Design, Vol. 47, No. 9, pp. 100-101 (Penton Publishing, Cleveland, Ohio, 1975).

15. E. B. Haugen and P. H. Wirshing, op. cit., p. 99.

16. A. A. Afifi and S. P. Azen, op. cit., pp. 86-98.

17. E. B. Haugen and P. H. Wirshing, op. cit., pp. 102-103.

18. A. A. Afifi and S. P. Azen, op. cit., pp. 317-318.

19. P. E. Pfeiffer, Concepts of Probability Theory, pp. 238-239.